Search for Rare and Forbidden Dilepton Decays of 4-particle decay modes of D^0

Eric Aitala, David Sanders

Abstract:

We report the results of a search for flavor-changing neutral-current (FCNC), lepton family violating (LFV) decays, and lepton number violating (LNV) decays of the 4-particle decay modes of D^0 (and their antiparticles) into modes containing muons and electrons. The results come from Fermilab charm hadroproduction experiment E791. We examined the resonant decay modes $D^0 \to \rho^0 \ell^\pm \ell^\mp$, $D^0 \to \overline{K}^{*0} \ell^\pm \ell^\mp$, and $D^0 \to \phi \ell^\pm \ell^\mp$ as well as the $D^0 \to \pi\pi\ell\ell$, $D^0 \to K\pi\ell\ell$, and $D^0 \to KK\ell\ell$ (both the opposite-sign and same-sign dileptons) decay modes. We present upper limits on the branching fractions at the 90% confidence level. These upper limits provide significant improvements over published results.

Offline_doc_434

Version 2.9

August 31, 2000

Table of Contents:

Introduction

This analysis is a continuation of work started by others in this collaboration (1,2, and 3). This current method uses a "blind" or "closed box" technique where first one optimizes the cuts while excluding the data signal region and then later one opens the "box". The starting point for this is the KSU substrip. The code for this analysis was a simple substrip of any 4-prong SESTR vertex that passes the minimum track quality stripping cuts and had a net charge of 0. The Ntuple program then took these 4-prongs vertices and applied particle ID to the tracks and fit the tracks to a D^0 mass window of $\pm$ 150 MeV/c2. Both resonant and all-track modes are in the Ntuples (the resonant mass is a Ntuple variable). For kaon-ID the track with the highest kaon Čerenkov probability was called a kaon, though we will eventually have to set some limit since we can not use the opposite sign as a tag. We plan to use modes with the same number of kaons as the normalization modes. That is $D^0 \to \pi^+\pi^-\pi^+\pi^-$ for $D^0 \to \rho^0 \ell^\pm \ell^\mp$ (and $D^0 \to \pi\pi\ell\ell$), $D^0 \to \overline{K}^{*0}\pi^+\pi^-$ for $D^0 \to \overline{K}^{*0}\ell^\pm\ell^\mp$ ($D^0 \to K^-\pi^+\pi^-\pi^+$ for $D^0 \to K\pi\ell\ell$), and $D^0 \to \phi\pi^+\pi^-$ for $D^0 \to \phi\ell^\pm\ell^\mp$ ($D^0 \to K^+K^-\pi^+\pi^-$ for $D^0 \to KK\ell\ell$). (We will examine the use of seed3 data for $D^0 \to K^-\pi^+\pi^-\pi^+$). We will use $D^0 \to \rho^0\pi^+\pi^-$ for $D^0 \to \rho^0\ell^\pm\ell^\mp$ if we can also determine the $D^0 \to \rho^0\pi^+\pi^-$ branching fraction. We plan to use the same muon[4] and electron ID as in the previous study, but we will investigate the use of the X-wall only tracks. To set the cuts we are using Monte Carlo "signal" and wing-data (outside the "box") background and then optimized the Monte Carlo "signal" versus the square root of the background e.g. $MC/\sqrt{Bkgnd}$.

The decay modes (and those of their antiparticles) that were examined are described in Table 1. See Figure 1, Figure 2 and Figure 3 for the Feynman Diagrams.

Table 1: Decay Modes Examined

FCNC	LFV	LNV
$D^0 \to \rho^0\mu^+\mu^-$	$D^0 \to \rho^0\mu^\pm e^\mp$	$D^0 \to \pi^-\pi^-\mu^+\mu^+$
$D^0 \to \rho^0 e^+e^-$	$D^0 \to \overline{K}^{*0}\mu^\pm e^\mp$	$D^0 \to \pi^-\pi^- e^+e^+$
$D^0 \to \overline{K}^{*0}\mu^+\mu^-$	$D^0 \to \phi\mu^\pm e^\mp$	$D^0 \to K^-\pi^-\mu^+\mu^+$
$D^0 \to \overline{K}^{*0}e^+e^-$	$D^0 \to \pi^+\pi^-\mu^\pm e^\mp$	$D^0 \to K^-\pi^- e^+e^+$
$D^0 \to \phi\mu^+\mu^-$	$D^0 \to K^-\pi^+\mu^\pm e^\mp$	$D^0 \to K^-K^-\mu^+\mu^+$
$D^0 \to \phi e^+e^-$	$D^0 \to K^+K^-\mu^\pm e^\mp$	$D^0 \to K^-K^- e^+e^+$
$D^0 \to \pi^+\pi^-\mu^+\mu^-$	$D^0 \to \pi^-\pi^-\mu^+e^+$	
$D^0 \to \pi^+\pi^- e^+e^-$	$D^0 \to K^-\pi^-\mu^+e^+$	
$D^0 \to K^-\pi^+\mu^+\mu^-$	$D^0 \to K^-K^-\mu^+e^+$	
$D^0 \to K^-\pi^+e^+e^-$		
$D^0 \to K^+K^-\mu^+\mu^-$		
$D^0 \to K^+K^-e^+e^-$		

History and Status

History

We started with the work from the two and three prong rare decays (Offline_doc_393) for the kinematic cuts. The muon and electron ID cuts will be the same as those used in the previous analysis (Offline_doc_393). The kinematic cuts were:

Offline_Doc_393 Final D^0 Cuts:

Mass window: $1.715 \text{ GeV/c}^2 < M(D^0) < 2.015 \text{ GeV/c}^2$
SDZ>12
DZTARG>5
TRKXIS<5
VITXIS<6
XYZVTX<-0.4 cm
τ<3 ps
DIP<0.040 mm
PTB<0.300 GeV/c
RATIO<0.01
"Box": (1.76)$1.83 \text{ GeV/c}^2 < M(D^0) < 1.90 \text{ GeV/c}^2$
K-Čerenkov Prob. >0.13 ($D^0 \rightarrow K^- \pi^+$)
EMPROB>90 (electrons)
mucat and *dist* from offline_doc_393 and 219 (see below) (muons)

Status

The status so far is that I:

- Generated Monte Carlo events for the modes described above.
- Filtered the Monte Carlo events using the KSU microstrip and the 4-prong substrip.
- Ran the 4-prong substrip on data from the KSU microstrip.
- Made cut for hole in the Čerenkov mirror midplane[5].
- Removed all category 3 tracks.
- Set asymmetric cuts at 1/2 the mass window width above and 3/2 the width below the mass for decays involving electrons to account for the bremsstrahlung tail, rather than 1/2 the width above and 1/2 the width below for dimuon decays. Because the bremsstrahlung tail sticks out of a symmetric "box" a solution must be found to preserve the method of "blind" analysis. My solution is to extend the lower limit of the mass window to cover the tail.
- Produced Ntuples of both Data and Monte Carlo based on the 4-prong substrip, using Chong's muon quality and distance cuts[3].
- Performed background studies of possible reflections/misidentifications of $K \rightarrow \pi(\ell)$.
- Performed background studies of possible reflections/misidentifications of $\pi \rightarrow \mu$(e).
- Determined if the normalization mode peaks, which are the sources of misidentified pions, are contained in the mass windows when pions are reflected as leptons, that is $\pi \rightarrow \mu$(e). For the $\mu\mu$

modes, 80% of the $D^0 \to K\pi\mu\mu$ modes and 90% of the $D^0 \to \pi\pi\mu\mu$ modes were contained within the "box". Adjustments were made to the misidentification rates in Table 15. The rest of the modes were all contained within the "boxes". (See Figure 10 for non-resonant modes and Figure 11 for resonant modes.)

- Checked the fits for estimated data shape using Monte Carlo plots. (See Figure 9.)
- I opened the DIP cut from <0.020 mm to <0.030mm.
- I decided that I should use a K-Čerenkov probability cut. I set this to >0.13 and increased the DIP cut to <0.040 mm (from <0.030mm). That is, with the sole exception of the $D^0 \to \phi \ell^+ \ell^-$ modes. There I decided that the ϕ-mass cut was strong enough and I will only increase the DIP cut to <0.040 mm.
- In attempting to explain why the Monte Carlo yield for $D^0 \to K^- K^- \mu^+ \mu^+$ relative to that of $D^0 \to K^- K^- e^+ e^+$ is about 50% while for $D^0 \to \phi \mu^+ \mu^-$ and $D^0 \to \phi e^+ e^-$ they have about the same yield I have compiled the following table of the number of Monte Carlo events left at various stages out of the original 250,000 Generated events. (I also observed a similar ratio for $D^0 \to K^+ K^- \mu^+ \mu^-$ and $D^0 \to K^+ K^- e^+ e^-$.)

Table 2: Relative Yields

Mode	Pass KSU Strip	Pass 4-prong Strip	Pass Ntuple tagging cuts	Pass Ntuple D^0-mass cut
$D^0 \to K^+ K^- \mu^+ \mu^-$	89980	3371	284	144
$D^0 \to K^+ K^- e^+ e^-$	75664	2567	369	267
$D^0 \to \phi \mu^+ \mu^-$	81013	2838	328	214
$D^0 \to \phi e^+ e^-$	73455	2393	364	236
$D^0 \to K^- K^- \mu^+ \mu^+$	82024	3246	252	117
$D^0 \to K^- K^- e^+ e^+$	74974	2613	386	258

In Table 2 the first 2 columns are the number of events that passed basic cuts, the basic vertex and track quality cuts ("Tagging cuts) for the KSU strip and simply any 4-prong (SEED3 or SEED4) for the 4-prong strip. The 3rd column is those events that pas my minimal kinematic cuts and are tagged as dileptons. These minimal kinematic cuts are: PTB<0.5 GeV/c, SDZ>10, DIP<0.100 mm, DZTARG>5, TRKXIS<5, VITXIS<6, τ<5 ps, RATIO<0.0005, and the midplane mirror cut. The lepton tagging cuts are EMPROB>80 for electrons and *mucat*>=3. The last column is the number of events that also are within 150 MeV/c^2 of the D^0 mass.

After examining every cut closely I noticed that there were a large number of 3 and 4 lepton events for the $D^0 \to KK\mu\mu$ modes, in fact there were more 3-lepton events than 2-lepton events. I first thought that this was kaons decaying-in-flight into muons. However, this effect was also seen for $D^0 \to K\pi\mu\mu$ and $D^0 \to \pi\pi\mu\mu$ modes. After further examination we found that with 4-prong events there was a reasonable likelihood that one of the non-muon tracks would point at a paddle that was hit in the muon wall. This was not seen in $D^0 \to KKee$ modes since, for Monte Carlo events, there were no hits in muon paddles. So we had a paddle-sharing problem. The solution was when tagging a track as a muon track, which shared a paddle with a previously tagged track, the track with the closest y-hit was called the muon. The closest hit was determined to be the hit with the least sigma in y or the one with the highest value of *mucat*. This seemed to mostly fix the problem for not only the $D^0 \to KK\mu\mu$ modes but all the other modes as well. This should also account for any real kaon decay-in-flight.

- I decided what should I use for the $D^0 \to K^- K^- \ell^+ \ell^+$ pion misidentification background rate. That is, what should I use for the number of $D^0 \to K^- K^- \pi^+ \pi^+$ events? Unless anyone comes up with a better idea I am just assuming that there are 0 misidentified pion events for these modes. This should be ok since this is a more conservative estimate.
- I checked what cuts Shiral had different for SEED3 and SEED4 vertices. He originally had a tighter SDZ for SEED3 (see Table 7) and used a cut on the maximum RATIO. I am not using a cut on the maximum RATIO and for the SDZ there were too few events to give significant results (see Table 8). Therefore I am not going to use separate cuts for SEED3 and SEED4 vertices.
- Changed the cut on NEWCATSG category 3 tracks to allow category 3 pions.
- Recalculated cuts using the non-resonant Monte Carlos.
- Studied the effect of excluding the *mucat*=3 muons. I found that there were no serious problems with the X-wall of the muon detectors.
- I re-examined the cut for hole in the Čerenkov mirror midplane and found that it removes about 10% of each normalization mode, $D^0 \to 4\pi$ as well as $D^0 \to K3\pi$ and $D^0 \to KK2\pi$. Therefore, I modified it to only apply to tracks that we are calling kaons.
- Checked the sources and calculations of the systematic errors.
- Following Alan's suggestion I decided to increase *K*-Čerenkov probability cut for modes containing only 1 kaon to >0.18.
- I slightly modified my algorithm that handles the paddle-sharing problem described above. What I did was rather than choosing the closest hit as follows: by determining it to be the hit with the least sigma in y or the one with the highest value of *mucat.* I decided to use the track with the highest value of *mucat* OR, when the value of *mucat* is the same, the hit with the least sigma in y. There was no apparent change but it seems to be a better algorithm.
- Opened the boxes. Calculated the pion-lepton misidentification rate based on the numbers of events found in the $D^0 \to K^+ \pi^- \mu^+ \mu^-$, $D^0 \to K^+ \pi^- e^+ e^-$, and $D^0 \to K^+ \pi^- \mu^\pm e^\mp$ modes.
- Decided that we should keep the SEED3 events (~7% of the total $D^0 \to K3\pi$ events). Since, for the $D^0 \to K^+ \pi^- \ell^+ \ell^-$ modes, there were 1/12, 1/6 and 2/15 events from SEED3 for the $D^0 \to K^+ \pi^- \mu^+ \mu^-$, $D^0 \to K^+ \pi^- e^+ e^-$, and $D^0 \to K^+ \pi^- \mu^\pm e^\mp$ modes, respectively.
- I corrected the systematic errors to account for the change in the calculation of the pion-lepton misidentification rate.
- Added functional plots of background and predicted data to plots. (See Figure 9.)
- Corrected systematic errors.

Things to do

- I calculated a resonant mass ρ for $D^0 \to \pi^+ \pi^- \pi^+ \pi^-$, but there are still some questions left before we can determine a Branching Fraction for $D^0 \to \rho^0 \pi^+ \pi^-$. These include what fraction of $D^0 \to \pi^+ \pi^- \pi^+ \pi^-$ are $D^0 \to \rho^0 \pi^+ \pi^-$, $D^0 \to \rho^0 \rho^0$, or non-resonant $D^0 \to \pi^+ \pi^- \pi^+ \pi^-$?

Cuts

Variable Definitions

SDZ: The significance of spatial separation from the primary vertex of the secondary vertex, along the beam direction.
DZTARG: The number of sigmas the secondary vertex is outside the target.
TRKXIS: The maximum of the fit χ^2 of the reconstructed tracks.
VITXIS: The maximum χ^2 fit of the reconstructed vertex.
XYZVTX: The position along the beam (z-coordinate) direction of the secondary vertex in cm.
τ: The lifetime of the parent particle, in picoseconds (ps).
PTB: The component of the parent particle momentum perpendicular to the line joining the primary and secondary vertices, in GeV/c.
DIP: The transverse impact parameter of the parent particle with respect to the primary vertex, in mm.
RATIO: The product, for each reconstructed track in the vertex, of the ratio of the distance between the track and the secondary vertex and of the distance between the track and the primary vertex. Set to $10^{-nprong}$ where nprong is the number of tracks/vertex.
EMPROB: The probability of that track being an electron in percent.
SIGMAS: The number of sigmas a projected muon track was from a hit ion the muon scintillator wall.
mucat: The muon track quality. See below under muon cuts.
dist: The "distance" from the center-line to the point $(x(cts), y(cm))$ in a plot of TDC counts (translated to "*x*") versus projected *y* position in units of approximately TDC counts. Also see below under muon cuts.
rmass: The mass of the resonant mode used.

Kinematics Cuts

The starting point for determining the kinematics cuts was the final cuts from Offline_Doc_393 (as given above). Any deviation will be underlined.

Offline_Doc_434 Final D^0 Cuts:

Mass window: $1.715\ \text{GeV}/c^2 < M(D^0) < 2.015\ \text{GeV}/c^2$
SDZ>12
DZTARG>5
TRKXIS<5
VITXIS<6
XYZVTX<-0.4 cm
<u>τ<2.5 ps</u>
<u>DIP<0.030 mm</u>
RATIO<0.0005
PTB<0.300 GeV/c
"Box": $(1.76)1.83\ \text{GeV}/c^2 < M(D^0) < 1.90\ \text{GeV}/c^2$
EMPROB>90 (electrons)
Mucat and *Dist* from offline_doc_393 and 219 (see below) (muons)

Due to low statistics I am summing the histograms used to determine the cuts, that is the sum of the $\mu\mu$, μe and ee modes for each resonance and the sum for all 3 resonance's. Each cut was varied with the other kinematic variable set to the offline_doc_393 levels.

The SDZ cut for the range from 10 to 15, using the summed histograms (with resonant cut).

Table 3: SDZ Results for D^0.

	SDZ>10	SDZ>11	SDZ>12	SDZ>13	SDZ>14	SDZ>15
$D^0 \rightarrow \rho^0 \ell^\pm \ell^\mp$:						
Monte Carlo	1034(1010)	1008(1002)	967(981)	945(961)	923(918)	881(889)
Background	7(2)	7(2)	7(2)	7(2)	7(2)	7(2)
$S/\sqrt{B}$	**391(714)**	381(709)	365(694)	357(679)	349(649)	333(629)
$D^0 \rightarrow \overline{K}^{*0} \ell^\pm \ell^\mp$:						
Monte Carlo	550(563)	529(545)	503(543)	485(520)	456(487)	454(468)
Background	43(9)	41(9)	37(9)	36(8)	33(8)	30(8)
$S/\sqrt{B}$	**84(188)**	83(182)	83(181)	81(184)	79(172)	83(165)
$D^0 \rightarrow \phi \ell^\pm \ell^\mp$:						
Monte Carlo	301(430)	291(415)	285(407)	275(397)	259(378)	253(357)
Background	36(2)	33(1)	28(0)	26(0)	23(0)	22(0)
$S/\sqrt{B}$	50	51	54	54	**54**	54
All:						
Monte Carlo	1885(2003)	1828(1962)	1755±42(1931)	1705(1878)	1638(1783)	1588(1714)
Background	86(13)	81(12)	72±8(11)	69(10)	63(10)	59(10)
$S/\sqrt{B}$	203(556)	203(566)	**207±13**(582)	205(**594**)	206(564)	207(542)

The DIP cut for the range from 0.060 to 0.010 mm, using the summed histograms (with resonant cut). I do not like the drop in the Monte Carlo numbers between 0.03 and 0.02 mm, I opted to use 0.04 mm rather than 0.02 mm for the DIP cut.

Table 4: DIP Results for D^0.

	DIP<0.06	DIP<0.05	DIP<0.04	DIP<0.03	DIP<0.02	DIP<0.01
$D^0 \rightarrow \rho^0 \ell^\pm \ell^\mp$:						
Monte Carlo	1029(1022)	1017(1014)	1014(990)	947(969)	793(790)	360(361)
Background	7(2)	7(2)	6(2)	5(2)	1(2)	1(2)
$S/\sqrt{B}$	389(**723)**	384(717)	414(700)	424(685)	**793**(559)	360(255)
$D^0 \rightarrow \overline{K}^{*0} \ell^\pm \ell^\mp$:						
Monte Carlo	532(567)	534(553)	537(552)	492(516)	403(406)	153163)
Background	43(9)	39(8)	35(6)	23(4)	12(1)	7(1)
$S/\sqrt{B}$	81(189)	86(196)	91(225)	103(258)	**116(406)**	58(163)
$D^0 \rightarrow \phi \ell^\pm \ell^\mp$:						
Monte Carlo	297(424)	293(424)	299(416)	270(383)	222(311)	86(146)
Background	36(2)	34(2)	30(2)	23(2)	13(1)	2(0)
$S/\sqrt{B}$	50(300)	50(300)	55(294)	56(271)	**62(311)**	61
All:						
Monte Carlo	1858(2013)	1844(1991)	1850±43(1958)	1709(1868)	1418±38(1507)	599(670)
Background	86(13)	80(12)	71±8(10)	51(8)	26±5(4)	10(3)
$S/\sqrt{B}$	200(558)	206(575)	219±14(619)	239(660)	**278±28(754)**	189(387)

The tau cut for the range from 5 to 1 ps, using the summed histograms (with resonant cut). Because the individual results ranged over most of the values and the total summed results are flat we will keep the value for τ<2.5 ps from the KSU stripper D^0 cuts.

Table 5: Tau Results for D^0.

	τ<5	**τ<4**	**τ<3**	**τ<2**	**τ<1**
$D^0 \to \rho^0 \ell^\pm \ell^\mp$:					
Monte Carlo	1028(1007)	1028(1035)	1018(912)	1009(986)	740(778)
Background	7(2)	7(2)	7(2)	7(2)	4(2)
$S/\sqrt{B}$	**389**(712)	**389(732)**	385(645)	381(697)	370(550)
$D^0 \to \overline{K}^{*0} \ell^\pm \ell^\mp$:					
Monte Carlo	547(563)	542(559)	550(558)	543(550)	390(407)
Background	43(9)	43(9)	43(9)	42(8)	21(5)
$S/\sqrt{B}$	84(188)	83(186)	84(186)	84**(194)**	**85**(182)
$D^0 \to \phi \ell^\pm \ell^\mp$:					
Monte Carlo	301(422)	296(429)	297(420)	287(413)	189(270)
Background	36(2)	36(2)	36(2)	34(2)	27(2)
$S/\sqrt{B}$	**50**(298)	49**(303)**	50(297)	49(292)	36(191)
All:					
Monte Carlo	1876(1992)	1866(2023)	1865(1890)	1839±43(1949)	1319(1455)
Background	86(13)	86(13)	86(13)	83±9(12)	52(9)
$S/\sqrt{B}$	202(552)	201(561)	201 (524)	**202±12(563)**	183(485)

The PTB cut for the range from 0.50 to 0.20 GeV/c, using the summed histograms (resonant cut).

Table 6: PTB Results for D^0.

	PTB<0.40	**PTB<0.35**	**PTB<0.30**	**PTB<0.25**	**PTB<0.20**
$D^0 \to \rho^0 \ell^\pm \ell^\mp$:					
Monte Carlo	1058(1000)	1030(988)	986(959)	929(905)	830(801)
Background	9(9)	7(8)	7(7)	7(7)	4(7)
$S/\sqrt{B}$	353(566)	389(640)	373(678)	350(699)	**415(707)**
$D^0 \to \overline{K}^{*0} \ell^\pm \ell^\mp$:					
Monte Carlo	553(560)	550(552)	535(512)	493(470)	446(439)
Background	50(2)	43(2)	34(2)	31(2)	26(1)
$S/\sqrt{B}$	78(187)	84**(195)**	**92**(194)	89(178)	87(166)
$D^0 \to \phi \ell^\pm \ell^\mp$:					
Monte Carlo	292(425)	301(420)	289(410)	274(392)	246(374)
Background	41(2)	36(2)	29(2)	25(2)	20(2)
$S/\sqrt{B}$	46(301)	50(297)	54(290)	55(277)	**55(374)**
All:					
Monte Carlo	1903(1985)	1881(1960)	1810±43(1881)	1693(1767)	1522(1614)
Background	100(13)	86(12)	70±8(11)	63(11)	50(10)
$S/\sqrt{B}$	190(551)	202(566)	**216±14(567)**	213(533)	215(510)

After applying the resonant mass cut, there was not much data left so the results lost any statistical significance. Therefore these kinematic cuts should not change. These cuts can be compared with Shiral's $D^0 \to K^- K^+ K^- \pi^+$ and the $D^0 \to K^- K^+ \pi^- \pi^+$ analysis cuts in the following table.

Table 7: Comparison of final cuts for 4-body D^0 decays.

Cut	$D^0 \to K^- K^+ \pi^- \pi^+$	$D^0 \to K^- K^+ K^- \pi^+$	4-prong Rare Decays
SDZ	>10(>14 SEED3)	>10 (>12 SEED3)	>12
DIP	<0.035 mm	<0.060 mm	<0.040 mm
PTB	<0.30 GeV/c(<0.35 SEED3)	<0.25 GeV/c	<0.30 GeV/c
Tau		<3.5 ps	<2.5 ps
K-Čerenkov prob.	>0.20(>0.3 SEED3)	>0.20	>0.13

To compare the difference between SEED3 and SEED4 events we recalculated the SDZ cut for the range from 10 to 15, using the summed histograms. Shown are the results for SEED4 and (SEED3).

Table 8: SEED4 and SEED3 SDZ Results for D^0.

	SDZ>10	**SDZ>11**	**SDZ>12**	**SDZ>13**	**SDZ>14**	**SDZ>15**
$D^0 \to \rho^0 \ell^\pm \ell^\mp$:						
Monte Carlo	1116(91)	1092(84)	1075(79)	1043(80)	1025(83)	1012(69)
Background	13(1)	13(1)	12(1)	12(1)	12(1)	12(1)
$S/\sqrt{B}$	310(91)	303(**84**)	**310(**79)	301(80)	296(83)	292(69)
$D^0 \to \overline{K}^{*0} \ell^\pm \ell^\mp$:						
Monte Carlo	604(55)	590(52)	579(50)	551(47)	544(42)	513(42)
Background	30(1)	29(1)	29(1)	28(1)	25(1)	24(0)
$S/\sqrt{B}$	**110**(**55**)	110(52)	108(50)	104(47)	109(42)	105
$D^0 \to \phi \ell^\pm \ell^\mp$:						
Monte Carlo	384(44)	373(41)	357(43)	346(39)	334(36)	334(32)
Background	26(4)	23(4)	20(3)	19(2)	18(2)	17(1)
$S/\sqrt{B}$	75(22)	78(21)	80(25)	79(28)	79(25)	**81**(**32**)
All:						
Monte Carlo	2104(190)	2055(177)	2011±45(172)	1940(166)	1903(161)	1859(143)
Background	69(6)	65(6)	61±8(5)	59(4)	55(4)	53(2)
$S/\sqrt{B}$	253(78)	255(72)	**257±17**(77)	253(83)	257(81)	255(**101**)

Because there was so little data in the SEED3 (about 7% of the $D^0 \to K^- \pi^+ \pi^- \pi^+$ signal) the results lost any statistical significance. Therefore we will not use separate cuts for SEED3 and SEED4 events.

For $D^0 \to K^- \pi^+ \ell\ell$ and $D^0 \to K^- \pi^+ \pi^- \pi^+$ modes I had to decide which particle was the kaon. To determine which particle is a kaon I set the mass of the particle with the largest K-Čerenkov probability to the kaon mass. For $D^0 \to K^- K^+ \pi^- \pi^+$ I chose the first kaon in this manner, then chose the opposite-signed particle that had the largest K-Čerenkov probability as the second kaon. For $D^0 \to K^- K^+ \ell\ell$ I just assumed that both hadrons were kaons. This applied to the resonant modes as well.

The cuts used on the mass of the resonant modes were determined from the width. They are:

rmass-ρ: $0.62\ \mathrm{GeV/c^2} < M(\rho) < 0.92\ \mathrm{GeV/c^2}$

rmass-$\overline{K}^{*0}$: $0.84\ \mathrm{GeV/c^2} < M(\overline{K}^{*0}) < 0.95\ \mathrm{GeV/c^2}$

rmass-ϕ: $1.01\ \mathrm{GeV/c^2} < M(\phi) < 1.03\ \mathrm{GeV/c^2}$ (Note the double width.)

For the cases where there was more than one possible combination that could produce the resonant state I calculated the value of *rmass* by taking the *rmass* closest to the resonant mass. Thus, for *rmass*-$\overline{K}^{*0}$, I picked the mass from the 2 possible $K^-\pi^+$ combinations that was closest to the $\overline{K}^{*0}$ mass. For the $D^0 \to \pi^+\pi^-\pi^+\pi^-$ mode I chose the closest of the 4 possible combinations.

I have plotted the masses of the resonant states for the lower background wing ($1.80 < M(D^0) < 1.83\ \mathrm{GeV/c^2}$), the central signal region ($1.83 < M(D^0) < 1.90\ \mathrm{GeV/c^2}$), and the upper background wing ($1.90 < M(D^0) < 1.93\ \mathrm{GeV/c^2}$) of the $D^0 \to \rho\pi^+\pi^-$, $D^0 \to \overline{K}^{*0}\pi^+\pi^-$, and $D^0 \to \phi\pi^-\pi^+$ normalization mode mass plots (See Figure 4).

Muon Cuts:

(All are from Offline_Doc_393 "Final Cuts", this subsection is here for reference only, though we do plan to look in to excluding *mucat*=3 tracks.)

There was a cut on the muon track momentum of $|\mathbf{P}_\mu|$>8 GeV/c and, for dimuon events, no two muon tracks may share the same Y-paddle.

The recommended cuts from Offline_Doc_219 were *mucat* = 3 or (*mucat* ≥ 6 and *dist* <10.0).

Muon Quality Category

To generate the following table, one starts with good muon candidates, that is a TDC hit in either a X or Y-Paddle or both a X and Y-Paddle, but only one hit per X or Y. A hit is defined as when a muon candidate track is projected to hit within a candidate paddle. The number of sigma is the distance of a projected track from the candidate paddle edge divided by the muon multiple scattering distance (from the calorimeters, steel and concrete). The variable *mucat* (muon category) is thus illustrated (the boldface numbers are the ones being used) in Table 9. The full text of the subroutine used to calculate *mucat* and *dist* can be found in the Appendix of offline_doc_393.

Table 9: mucat, the Muon Quality Category

y-hit \ x-hit	Hit X-Paddle	$\leq 1\sigma_x$	$>1\sigma_x$
Hit Y-Paddle	**9**	**8**	**7**
$\leq 1\sigma_y$	**6**	5	4
$>1\sigma_y$	**3**, 2	1	0

To check the muon quality categories for $D^+ \to \pi^+ \mu^+ \mu^-$ with different cuts in order to determine the best categories to use and determine what information from the X-wall is useable I used a series of cuts. The different cuts I used are:

(1) *dist* <10 cut on first muon, the offline_doc_219 final muon category cuts on second muon, and the final kinematics cuts,
(2) no *dist* cut on first muon, the offline_doc_219 final muon category cuts on second muon, and the final kinematics cuts,
(3) *dist* <10 cut on first muon, the offline_doc_219 final muon category cuts on second muon, and loose kinematics cuts,
(4) no *dist* cut on first muon, the offline_doc_219 final muon category cuts on second muon, and loose kinematics cuts,
(5) *dist* <10 cut on first muon, any muon category cuts on second muon, and loose kinematics cuts,
(6) no *dist* cut on first muon, any muon category cuts on second muon, and loose kinematics cuts,
(7) Chong's $K^{*0}\mu^+\nu_\mu$ data from offline_doc_219.

The $D^+ \to \pi^+ \mu^+ \mu^-$ Monte Carlo and data numbers for different cuts are given Table 10:

Table 10: Muon Quality Category								
Cut		**9**	**8**	**7**	**6**	**5**	**4**	**3**
(1)	MC	1993	161	245	444	48	62	293
	data	17	2	17	6	1	10	6
	$MC/\sqrt{B}$	483	114	59	181	48	20	120
(2)	MC	2000	161	248	445	48	66	293
	data	19	2	26	10	1	25	6
	$MC/\sqrt{B}$	459	114	49	141	48	13	120
(3)	MC	2681	229	328	589	70	87	395
	data	31	2	29	17	4	23	17
	$MC/\sqrt{B}$	482	162	61	143	35	18	96
(4)	MC	2690	230	333	590	70	94	395
	data	36	2	44	21	4	51	17
	$MC/\sqrt{B}$	448	163	50	129	35	13	96
(5)	MC	2778	241	339	612	73	88	413
	data	56	3	60	23	6	46	32
	$MC/\sqrt{B}$	372	139	44	128	30	13	73
(6)	MC	2798	242	344	613	73	95	413
	data	66	4	105	35	6	96	32
	$MC/\sqrt{B}$	344	121	34	104	30	10	73
(7)	RS	728	56	727	345	72	822	228
	WS	142	17	375	146	42	489	85
	$(RS-WS)/\sqrt{WS}$	49	9	18	16	5	15	16

One should note that the X-wall is roughly 10’ x 20’ and the Y-wall is only roughly 8’ x 10’. Therefore, we need to consider the *mucat*=3 tracks.

I then combined these categories for the some of the cuts described above and a:

(8) combination of Monte Carlo “signal” from cut (1) with “data” which is the same Monte Carlo “signal” weighted with the ratio of WS/RS from cut (7).

The resulting “signal-to-noise” ratios are given in Table 11:

Table 11: Muon Quality Category

Cut		3-9	3, 6-9	6-9	3, 7-9	7-9	6-9, 4, 3
(1)	MC	3251	3141±56	2847	2696	2402	3203
	data	59	48±7	42	42	36	58
	$MC/\sqrt{B}$	423	**453±34**	439	416	400	421
(6)	MC	4578	4410±66	3997	3797	3384	4505
	data	344	242±16	210	207	175	338
	$MC/\sqrt{B}$	247	**283±10**	276	264	256	245
(8)	MC	3251	3141±56	2847	2696	2402	3203
	“data”	927	863±29	753	674	565	900
	$MC/\sqrt{B}$	107	**107±3**	104	104	101	107
(7)	RS	2978	2084±46	1856	1739	1511	2906
	WS	1296	765±28	680	619	534	1254
	$(\mathrm{RS}-\mathrm{WS})/\sqrt{\mathrm{WS}}$	47	**48±1**	45	45	42	47

As one can see, the original muon category cuts determined in offline_doc_219 are the best cuts; therefore, for this analysis they are the final cuts to be used.

Where $dist = \left| \frac{(m \cdot \mathrm{tdc}_{\mu} + b) - X_{\mathrm{Proj}}}{\sqrt{m^2+1}} \right|$ in units of ~10 cm and *m* is the slope and *b* the intercept for the global TDCs and when:

- Run Number < 1000, *m*=-9.8, *b*=9011
- 1000 ≤ Run Number < 1400, *m*=-10.0, *b*=9150
- Run Number ≥ 1400, *m*=-9.8, *b*=8971

To determine the TDC cut, *dist*, I tested it using background data and Monte Carlo events for the $D^+ \to \pi^+ \mu^+ \mu^-$ decay mode. Table 12 shows the results for 7 values of *dist*.

Table 12: Muon TDC Distance Cuts

Cut		***dist*<10**	***dist*<8**	***dist*<6**	***dist*<5.5**	***dist*<5**	***dist*<4.5**	***dist*<4**
Tight: (1) above, except *mucat*>6 cut on first muon	MC	3161	3132	3075±55	3050	3004	2915	2814
	data	22	21	17±4	17	16	16	16
	$MC/\sqrt{B}$	674	684	746±91	740	**751**	729	704
Loose: (6) above except *mucat*>6 cut on first muon	MC	4668	4662	5444±74	4502	4432	4307	4167
	data	115	101	88±9	79	75	72	71
	$MC/\sqrt{B}$	435	464	**580±32**	507	512	508	495

Given these results I will set the TDC *dist* cut at *dist*<6, a cut of 60 cm in spatial coordinates.

The Monte Carlo program mistakenly defined the muon X-wall efficiencies as 100% and not the 69% measured[6]. This discrepancy can be corrected for because the individual category is available for each muon track. The correction would involve weighting the each of muon category 6 and 3 tracks by the true efficiency (69%) for the Monte Carlo events with muon tracks. This is about a 10-15% effect.

Monte Carlo Studies

The number of Monte Carlo events generated and passing cuts is shown in the following table.

Table 13: Monte Carlo Yields

Mode	# Generated	# Passed Cuts	% Yield
$D^0 \to \pi^+\pi^-\pi^+\pi^-$	250,000	2383	0.95
$D^0 \to \pi^+\pi^-\mu^+\mu^-$	250,000	840	0.34
$D^0 \to \pi^+\pi^-e^+e^-$	250,000	345	0.14
$D^0 \to \pi^+\pi^-\mu^\pm e^\mp$	250,000	620	0.25
$D^0 \to K^-\pi^+\pi^-\pi^+$	250,000	1026	0.41
$D^0 \to K^-\pi^+\mu^+\mu^-$	250,000	286	0.11
$D^0 \to K^-\pi^+e^+e^-$	250,000	135	0.05
$D^0 \to K^-\pi^+\mu^\pm e^\mp$	250,000	217	0.09
$D^0 \to K^-K^+\pi^-\pi^+$	250,000	639	0.26
$D^0 \to K^+K^-\mu^+\mu^-$	250,000	145	0.06
$D^0 \to K^+K^-e^+e^-$	250,000	120	0.05
$D^0 \to K^+K^-\mu^\pm e^\mp$	250,000	149	0.06
$D^0 \to \rho\pi^+\pi^-$	250,000	2246	0.90
$D^0 \to \rho^0\mu^+\mu^-$	250,000	694	0.28
$D^0 \to \rho^0 e^+e^-$	250,000	294	0.12
$D^0 \to \rho^0\mu^\pm e^\mp$	250,000	466	0.19
$D^0 \to \overline{K}^{*0}\pi^+\pi^-$	250,000	694	0.28
$D^0 \to \overline{K}^{*0}\mu^+\mu^-$	250,000	275	0.11
$D^0 \to \overline{K}^{*0}e^+e^-$	250,000	121	0.05
$D^0 \to \overline{K}^{*0}\mu^\pm e^\mp$	250,000	185	0.07
$D^0 \to \phi\pi^-\pi^+$	250,000	535	0.21
$D^0 \to \phi\mu^+\mu^-$	250,000	187	0.07
$D^0 \to \phi e^+e^-$	250,000	117	0.05
$D^0 \to \phi\mu^\pm e^\mp$	250,000	146	0.06
$D^0 \to \pi^-\pi^-\mu^+\mu^+$	250,000	821	0.33
$D^0 \to \pi^-\pi^-e^+e^+$	250,000	322	0.13
$D^0 \to \pi^-\pi^-\mu^+e^+$	250,000	559	0.22
$D^0 \to K^-\pi^-\mu^+\mu^+$	250,000	268	0.11
$D^0 \to K^-\pi^-e^+e^+$	250,000	134	0.05
$D^0 \to K^-\pi^-\mu^+e^+$	250,000	238	0.10
$D^0 \to K^-K^-\mu^+\mu^+$	250,000	137	0.05
$D^0 \to K^-K^-e^+e^+$	250,000	137	0.05
$D^0 \to K^-K^-\mu^+e^+$	250,000	175	0.07

See Figure 5 for the Monte Carlo decay modes without the resonant mass cut, Figure 6 for the Monte Carlo decay modes with the resonant mass cut, Figure 7 for the Monte Carlo modes with same-sign dileptons, and Figure 8 for the Monte Carlo normalization modes.

Background Studies

Reflection Background

To examine possible reflections from normal charm hadron decays for the dilepton modes, the tracks were refit with deliberately wrong particle mass for each event. This produced a “reflection” into one of the following possible hadron decays:

(1) $D^0 \to \pi^+\pi^-\pi^+\pi^-$ with a mass window of $1.83\ \text{GeV/c}^2 < M(D^0) < 1.90\ \text{GeV/c}^2$

(2) $D^0 \to K^-\pi^+\pi^-\pi^+$ with a mass window of $1.83\ \text{GeV/c}^2 < M(D^0) < 1.90\ \text{GeV/c}^2$

(3) $D^0 \to K^-K^+\pi^-\pi^+$ with a mass window of $1.83\ \text{GeV/c}^2 < M(D^0) < 1.90\ \text{GeV/c}^2$

Then the event was tagged if they were within a mass window of the proposed reflections. The percentage of tagged events for each decay mode is shown in Table 14.

Table 14: The percentage of events that are within the mass window of the reflections.

Reflection Mode	$D^0 \to \pi^+\pi^-\pi^+\pi^-$		$D^0 \to K^-\pi^+\pi^-\pi^+$		$D^0 \to K^-K^+\pi^-\pi^+$	
	MC	**Data**	**MC**	**Data**	**MC**	**Data**
$D^0 \to \rho^0\mu^+\mu^-$	83%	0%	2%	50%	0	0%
$D^0 \to \rho^0 e^+e^-$	37%	100	1%	0%	0	0%
$D^0 \to \rho^0\mu^\pm e^\mp$	54%	0	1%	0	0	0
$D^0 \to \overline{K}^{*0}\mu^+\mu^-$	1%	0	50%	33%	1%	17%
$D^0 \to \overline{K}^{*0} e^+e^-$	3%	0%	31%	0%	1%	0%
$D^0 \to \overline{K}^{*0}\mu^\pm e^\mp$	8%	0%	36%	0%	0	50%
$D^0 \to \phi\mu^+\mu^-$	0%	0	6%	0	92%	0
$D^0 \to \phi e^+e^-$	0	0	7%	0	33%	0
$D^0 \to \phi\mu^\pm e^\mp$	0	0	3%	0	42%	0

The conclusion from examining these results is that we should not cut events with the same number of kaons but that we should cut events with a different number of kaons. That is:

- For $D^0 \to \rho^0\ell^\pm\ell^\mp$ events, all reflections except $D^0 \to \pi^+\pi^-\pi^+\pi^-$ should be cut.
- For $D^0 \to \overline{K}^{*0}\ell^\pm\ell^\mp$ events, all reflections except $D^0 \to K^-\pi^+\pi^-\pi^+$ should be cut.
- For $D^0 \to \phi\,\ell^\pm\ell^\mp$ events, all reflections except $D^0 \to K^-K^+\pi^-\pi^+$ should be cut.

Pion Misidentification Background

For this analysis we first planned to use the same misidentification rates determined in offline_doc_393. The following is included for reference.

To examine background from a π misidentified as a μ (or e) we did the following:

We decided to use the $D^+ \to K^- \ell^+ \ell^+$ modes to set a conservative misidentification rate for the other modes. The rate was determined first by counting the number of $D^+ \to K^- \ell^+ \ell^+$ events within the "box", then subtracting the flat background calculated from the background events outside of the "box" and finally by dividing the results by the number of $D^+ \to K^- \pi^+ \pi^+$ normalization events. This gave the misidentification rate of 13/17730 for $\pi\pi \to \mu\mu$, 6/17730 for $\pi\pi \to ee$, and 5.2/17730 for $\pi\pi \to \mu e$. The number of fitted events from the specific misidentification sources then multiplied this rate.

Then, rather than use the rates from offline_doc_393, we decided to first open the $D^0 \to K^+ \pi^- \mu^+ \mu^-$, $D^0 \to K^+ \pi^- e^+ e^-$, and $D^0 \to K^+ \pi^- \mu^\pm e^\mp$ modes. For these modes we would then use the smaller of the offline_doc_393 rates or, similar to the method described above, assume that the number of observed events were all from pion-lepton misidentification. For all the other modes we would use the rate from the assumption that the events observed for the $D^0 \to K^+ \pi^- \mu^+ \mu^-$, $D^0 \to K^+ \pi^- e^+ e^-$, and $D^0 \to K^+ \pi^- \mu^\pm e^\mp$ modes were all from pion-lepton misidentification. We observed 12, 6, and 15 events for the $D^0 \to K^+ \pi^- \mu^+ \mu^-$, $D^0 \to K^+ \pi^- e^+ e^-$, and $D^0 \to K^+ \pi^- \mu^\pm e^\mp$ modes, respectively. Therefore, the new pion-lepton misidentification rates, after subtracting combinatoric and long-range backgrounds and taking into account the factor of 2 due to combinatorics are: 3.96/11550 for $\pi\pi \to \mu\mu$, 1.04/11550 for $\pi\pi \to ee$, and 4.88/11550 for $\pi\pi \to \mu e$.

Unfortunately the likely sources of pion misidentification errors are the normalization modes themselves. Thus the fitted numbers are 2049±52.54 for $D^0 \to \pi^+ \pi^- \pi^+ \pi^-$, 11550±112.9 for $D^0 \to K^- \pi^+ \pi^- \pi^+$, 405.7±40.96 for $D^0 \to K^- K^+ \pi^- \pi^+$, 1954±5039 for $D^0 \to \rho^0 \pi^+ \pi^-$, 4917±72.10 for $D^0 \to \overline{K}^{*0} \pi^+ \pi^-$, and 101.6±16.40 for $D^0 \to \phi \pi^+ \pi^-$. For the cases of $D^0 \to \pi^+ \pi^- \ell^+ \ell^-$ the rate was quadrupled since there are four ways of getting then from $D^0 \to \pi^+ \pi^- \pi^+ \pi^-$. For the cases of $D^0 \to K^- \pi^+ \ell^- \ell^+$ the rate was doubled as for modes like $D^+ \to \pi^+ \pi^- \pi^+$ from Offline_doc_393.ps. There should not be any double counting for $D^0 \to \rho^0 \ell^+ \ell^-$, $D^0 \to \overline{K}^{*0} \pi^+ \pi^-$, and $D^0 \to \phi \pi^+ \pi^-$ modes. For $D^0 \to \pi^- \pi^- \ell^+ \ell^+$ and $D^0 \to K^- \pi^- \ell^+ \ell^+$ modes I will use $D^0 \to \pi^+ \pi^- \pi^+ \pi^-$ and $D^0 \to K^- \pi^+ \pi^- \pi^+$ respectively. For $D^0 \to K^- K^- \ell^+ \ell^+$ mode I will use 0 since there is no branching fraction for $D^0 \to K^- K^- \pi^+ \pi^+$. I have investigated whether or not the modes with doubly misidentified pions are still all contained within the "boxes". This was true for the $D^0 \to \pi^+ \pi^-$ modes but I was not sure if it is still true for these 4-prong modes. Unfortunately only 80% of the $D^0 \to K\pi\mu\mu$ modes and 90% of the $D^0 \to \pi\pi\mu\mu$ modes were contained within the "box". (See Figure 10 and Figure 11.) The number of misidentification background events from these calculations is given in Table 15.

Combinatoric and Long-Range Background

The number of combinatoric background events are determined from the closed "box" data shown in Figure 12, Figure 13, and Figure 14. They are calculated using the following algorithm: If there are events in the upper wings then assume a flat distribution, but if there are only events in the lower wings then assume 0 combinatoric background for those modes. The results are given in Table 15.

There is also some real long-range backgrounds to the $D^0 \to K^- \pi^+ \ell^- \ell^+$, $D^0 \to K^+ K^- \ell^+ \ell^-$, $D^0 \to \overline{K}^{*0} \ell^+ \ell^-$, and $D^0 \to \phi \ell^+ \ell^-$ decay modes. The source of this background are the $D^0 \to K^- \pi^+ \rho^0$, $D^0 \to K^+ K^- \rho^0$, $D^0 \to \overline{K}^{*0} \rho^0$, and $D^0 \to \phi \rho^0$ decay modes, respectively, where $\rho^0 \to \ell^+ \ell^-$ (either $\rho^0 \to \mu^+ \mu^-$ or $\rho^0 \to e^+ e^-$). This number is the product of Branching Fractions and the number of normalizing decays. In example for $D^0 \to \overline{K}^{*0} \ell^+ \ell^-$:

$$N_{LR}(D^0 \to \overline{K}^{*0} \ell^+ \ell^-) = \frac{BF(D^0 \to \overline{K}^{*0} \rho^0) \cdot BF(\rho^0 \to \ell^+ \ell^-)}{BF(D^0 \to \overline{K}^{*0} \pi^+ \pi^-)} \cdot N(D^0 \to \overline{K}^{*0} \pi^+ \pi^-). \qquad (1)$$

The expected long-range background numbers are given in Table 15.

Table 15: Number of Background Events

Mode	**Combinatoric**	**# mis-ID**	**Long-ranged**	**Total**
$D^0 \to \pi^+ \pi^- \mu^+ \mu^-$	0.00	3.16		3.16
$D^0 \to \pi^+ \pi^- e^+ e^-$	0.00	0.73		0.73
$D^0 \to \pi^+ \pi^- \mu^\pm e^\mp$	5.25	3.46		8.71
$D^0 \to K^- \pi^+ \mu^+ \mu^-$	3.65	7.91	0.440	12.00
$D^0 \to K^- \pi^+ e^+ e^-$	3.50	2.07	0.430	6.00
$D^0 \to K^- \pi^+ \mu^\pm e^\mp$	5.25	9.75		15.00
$D^0 \to K^+ K^- \mu^+ \mu^-$	2.13	0.17	0.067	2.37
$D^0 \to K^+ K^- e^+ e^-$	6.13	0.04	0.066	6.23
$D^0 \to K^+ K^- \mu^\pm e^\mp$	3.50	0.17		3.67
$D^0 \to \rho^0 \mu^+ \mu^-$	0.00	0.75		0.75
$D^0 \to \rho^0 e^+ e^-$	0.00	0.18		0.18
$D^0 \to \rho^0 \mu^\pm e^\mp$	0.00	0.82		0.82
$D^0 \to \overline{K}^{*0} \mu^+ \mu^-$	0.30	1.68	0.233	2.22
$D^0 \to \overline{K}^{*0} e^+ e^-$	0.88	0.44	0.228	1.54
$D^0 \to \overline{K}^{*0} \mu^\pm e^\mp$	1.75	2.08		3.83
$D^0 \to \phi \mu^+ \mu^-$	0.30	0.04	0.003	0.35
$D^0 \to \phi e^+ e^-$	0.00	0.01	0.003	0.01
$D^0 \to \phi \mu^\pm e^\mp$	0.00	0.05		0.05
$D^0 \to \pi^- \pi^- \mu^+ \mu^+$	0.91	0.79		1.70
$D^0 \to \pi^- \pi^- e^+ e^+$	0.00	0.18		0.18
$D^0 \to \pi^- \pi^- \mu^+ e^+$	2.63	0.86		3.49
$D^0 \to K^- \pi^- \mu^+ \mu^+$	2.74	3.96		6.69
$D^0 \to K^- \pi^- e^+ e^+$	0.88	1.04		1.91
$D^0 \to K^- \pi^- \mu^+ e^+$	0.00	4.88		4.88
$D^0 \to K^- K^- \mu^+ \mu^+$	1.22	0.00		1.22
$D^0 \to K^- K^- e^+ e^+$	0.88	0.00		0.88
$D^0 \to K^- K^- \mu^+ e^+$	0.00	0.00		0.00

Results

General Method

$$BR_X = \frac{N_X/\varepsilon_X}{N_{\text{norm.}}/\varepsilon_{\text{norm.}}} \cdot BR_{\text{norm.}} = \frac{N_X}{N_{\text{norm.}}} \cdot \frac{\varepsilon_{\text{norm.}}}{\varepsilon_X} \cdot BR_{\text{norm.}} \qquad (2)$$

Where $\frac{\varepsilon_{\text{norm.}}}{\varepsilon_X} = \frac{N^{MC}_{\text{norm.}}}{N^{MC}_X}$ (3)

Example for $D^0 \to K^{*0} e^+ e^-$

For $D^0 \to K^{*0} e^+ e^-$: $\frac{\varepsilon_{K^{*0}\pi\pi}}{\varepsilon_{K^{*0}e^+e^-}} = \frac{N^{MC}_{K^{*0}\pi\pi}}{N^{MC}_{K^{*0}e^+e^-}} = \frac{694}{121} = 5.735$.

For a 90% CL Upper Limit one observes the number of events in the box, takes predicted background level and using the 90% CL table[7], $\frac{N_{K^{*0}e^+e^-}}{N_{K^{*0}\pi\pi}} < \frac{N_{90\%\ \text{CL.}}}{4917} = \frac{4.37}{4917}$ therefore $BR_{K^{*0}e^+e^-} < 5.10 \times 10^{-3} \cdot BR_{K^{*0}\pi\pi}$ (90% CL). Thus: $BR_{K^{*}e^+e^-} < 4.84 \times 10^{-5}$ (90% CL).

Systematic Errors

The value N_x in Equation (1) must be corrected for systematic errors. To do this we use the method described in Cousins and Highland[8] (Eqn. 20). In this equation $N_x = U_x + \Delta U_x$ where U_x is the uncorrected value of N_x that is calculated from the table using the method of Feldman and Cousins[6]. And

$$\Delta U_x = \frac{U_x + B - n}{U_x + B} \cdot \frac{U_x^2 \sigma_r^2}{2} \qquad (2)$$

where B is the predicted background and σ_r is the total systematic errors.

The sources of the systematic errors are given, as a fraction, in Table 16 as follows:

1) Normalization fit. This is the error from paw fits, i.e. ±52.64/2049 from Figure 15.
2) Normalization Branching Ratio from the 2000 PDG.
3) Monte Carlo statistics of the normalization mode. Simply $1/\sqrt{N}$ from the column labeled "# Passed Cuts" in Table 13.
4) Monte Carlo statistics of the decay mode. Simply $1/\sqrt{N}$ as in (3).
5) Misidentification background. This includes statistical errors in the fit as in (1) above of the normalization modes such as $D^0 \to \overline{K}^{*0} \pi^+ \pi^-$ and in the number of $D^+ \to K^- \pi^+ \pi^+$ used in the calculation of the misidentification rate. It also includes differences between a flat fit and exponential fit of the combinatorial background and errors in the determination of the number of events in the $D^+ \to K^- \ell^+ \ell^+$ modes.
6) Particle ID efficiency, including hodoscope efficiencies – Muon Y-wall (99±1%) and X-wall (69±3%) and ±5% for electron identification [9, 10].
7) Tails. This is calculated as 25% of the fraction, ε_X, of Monte Carlo events that remain outside of the "box", divided by the fraction, 1-ε_X, that remains within the "box". Where ε_X is the difference in the

number of events between the shaded regions and the full plot, divided by the number of events in the full plot for each plot in Figure 6.

8) Resonant mode Branching ratio. This is the difference between the fitted numbers of $D^0 \to \pi^+\pi^-\pi^+\pi^-$ and $D^0 \to \rho^0\pi^+\pi^-$ divided by the fitted number of $D^0 \to \pi^+\pi^-\pi^+\pi^-$.

It should be noted that sources 6-8 could be lumped together as "Tagging Errors".

Table 16: The systematic errors.

Mode	1	2	3	4	5	7	8	9	Total
$D^0 \to \pi^+\pi^-\mu^+\mu^-$	0.026	0.068	0.021	0.035	0.074	0.014	0.008		0.113
$D^0 \to \pi^+\pi^- e^+e^-$	0.026	0.068	0.021	0.054	0.043	0.050	0.020		0.116
$D^0 \to \pi^+\pi^-\mu^\pm e^\mp$	0.026	0.068	0.021	0.040	0.114	0.037	0.015		0.148
$D^0 \to K^-\pi^+\mu^+\mu^-$	0.010	0.041	0.021	0.059	0.133	0.014	0.031		0.157
$D^0 \to K^-\pi^+ e^+e^-$	0.010	0.041	0.021	0.086	0.195	0.050	0.043		0.228
$D^0 \to K^-\pi^+\mu^\pm e^\mp$	0.010	0.041	0.021	0.068	0.120	0.037	0.039		0.155
$D^0 \to K^+K^-\mu^+\mu^-$	0.101	0.092	0.043	0.083	0.006	0.014	0.034		0.170
$D^0 \to K^+K^- e^+e^-$	0.101	0.092	0.043	0.091	0.003	0.050	0.019		0.178
$D^0 \to K^+K^-\mu^\pm e^\mp$	0.101	0.092	0.043	0.082	0.003	0.037	0.007		0.169
$D^0 \to \rho^0\mu^+\mu^-$	0.026	0.068	0.021	0.038	0.022	0.014	0.005	0.046	0.101
$D^0 \to \rho^0 e^+e^-$	0.026	0.068	0.021	0.058	0.019	0.050	0.027	0.046	0.122
$D^0 \to \rho^0\mu^\pm e^\mp$	0.026	0.068	0.021	0.046	0.015	0.037	0.017	0.046	0.109
$D^0 \to \overline{K}^{*0}\mu^+\mu^-$	0.015	0.221	0.021	0.060	0.033	0.014	0.003		0.233
$D^0 \to \overline{K}^{*0} e^+e^-$	0.015	0.221	0.021	0.091	0.046	0.050	0.027		0.251
$D^0 \to \overline{K}^{*0}\mu^\pm e^\mp$	0.015	0.221	0.021	0.074	0.021	0.037	0.004		0.238
$D^0 \to \phi\mu^+\mu^-$	0.164	0.264	0.043	0.073	0.001	0.014	0.000		0.322
$D^0 \to \phi e^+e^-$	0.164	0.264	0.043	0.092	0.002	0.050	0.006		0.331
$D^0 \to \phi\mu^\pm e^\mp$	0.164	0.264	0.043	0.083	0.002	0.037	0.012		0.327
$D^0 \to \pi^-\pi^-\mu^+\mu^+$	0.026	0.068	0.021	0.035	0.019	0.014	0.005		0.087
$D^0 \to \pi^-\pi^- e^+e^+$	0.026	0.068	0.021	0.056	0.020	0.050	0.016		0.110
$D^0 \to \pi^-\pi^-\mu^+e^+$	0.026	0.068	0.021	0.042	0.013	0.037	0.020		0.097
$D^0 \to K^-\pi^-\mu^+\mu^+$	0.010	0.041	0.021	0.061	0.045	0.014	0.025		0.094
$D^0 \to K^-\pi^- e^+e^+$	0.010	0.041	0.021	0.086	0.114	0.050	0.035		0.163
$D^0 \to K^-\pi^-\mu^+e^+$	0.010	0.041	0.021	0.065	0.059	0.037	0.024		0.109
$D^0 \to K^-K^-\mu^+\mu^+$	0.101	0.092	0.043	0.085	0.000	0.014	0.005		0.167
$D^0 \to K^-K^- e^+e^+$	0.101	0.092	0.043	0.085	0.000	0.050	0.007		0.174
$D^0 \to K^-K^-\mu^+e^+$	0.101	0.092	0.043	0.076	0.000	0.037	0.013		0.167

Data

Table 17: Data

Mode	Predicted Background	Observed	90% CL Upper Limit[8]	90% CL Sys Err Corr[9]
$D^0 \to \pi^+\pi^-\mu^+\mu^-$	3.16	2.00	2.92	2.96
$D^0 \to \pi^+\pi^- e^+e^-$	0.73	9.00	14.57	15.16
$D^0 \to \pi^+\pi^-\mu^\pm e^\mp$	8.71	1.00	1.05	1.06
$D^0 \to K^-\pi^+\mu^+\mu^-$	12.00	12.00	7.00	7.23
$D^0 \to K^-\pi^+ e^+e^-$	6.00	6.00	5.47	5.84
$D^0 \to K^-\pi^+\mu^\pm e^\mp$	15.00	15.00	7.52	7.75
$D^0 \to K^+K^-\mu^+\mu^-$	2.37	0.00	1.20	1.22
$D^0 \to K^+K^- e^+e^-$	6.23	9.00	9.07	9.61
$D^0 \to K^+K^-\mu^\pm e^\mp$	3.67	5.00	6.32	6.61
$D^0 \to \rho^0\mu^+\mu^-$	0.75	0.00	1.78	1.80
$D^0 \to \rho^0 e^+e^-$	0.18	1.00	4.18	4.28
$D^0 \to \rho^0\mu^\pm e^\mp$	0.82	1.00	3.54	3.60
$D^0 \to \overline{K}^{*0}\mu^+\mu^-$	2.22	3.00	5.20	5.64
$D^0 \to \overline{K}^{*0} e^+e^-$	1.54	2.00	4.37	4.77
$D^0 \to \overline{K}^{*0}\mu^\pm e^\mp$	3.83	9.00	11.47	13.01
$D^0 \to \phi\mu^+\mu^-$	0.35	0.00	2.10	2.33
$D^0 \to \phi e^+e^-$	0.01	0.00	2.43	2.75
$D^0 \to \phi\mu^\pm e^\mp$	0.05	0.00	2.40	2.71
$D^0 \to \pi^-\pi^-\mu^+\mu^+$	1.70	1.00	2.76	2.78
$D^0 \to \pi^-\pi^- e^+e^+$	0.18	1.00	4.18	4.26
$D^0 \to \pi^-\pi^-\mu^+e^+$	3.49	4.00	5.11	5.18
$D^0 \to K^-\pi^-\mu^+\mu^+$	6.69	14.00	15.31	15.70
$D^0 \to K^-\pi^- e^+e^+$	1.91	2.00	4.00	4.14
$D^0 \to K^-\pi^-\mu^+e^+$	4.88	7.00	7.65	7.81
$D^0 \to K^-K^-\mu^+\mu^+$	1.22	1.00	3.16	3.27
$D^0 \to K^-K^- e^+e^+$	0.88	2.00	5.03	5.28
$D^0 \to K^-K^-\mu^+e^+$	0.00	0.00	2.44	2.52

See Figure 12 for the data decay modes without the resonant mass cut, Figure 13 for the data decay modes with the resonant mass cut, and Figure 14 for the data decay modes with same sign dileptons. See Figure 15 for the fitted normalization data modes, the upper plot is without the resonant mass cut and the middle plot is with the resonant mass cut applied, and the lower plot is the resonant masses used for the resonant mass cut. Note the large width of the $\rho^0 \to \pi^+\pi^-$ decay and the lack of previously measured branching fraction for $D^0 \to \rho\pi^+\pi^-$.

For the shape of the fitting functions, the moment, I started with those determined from the 2-prong $D^0 \to \ell^-\ell^+$ plots described in Offline_doc_393.ps. I used the new Monte Carlo events to refine the shapes. Note that this is only used to guide the eye, not to determine the number of observed events. The area under the curves will be set equal to the estimated 90% CL upper limit values, which will be corrected for systematic errors.

Preliminary Results

For all modes I then used this 90% CL upper limit predicted number of events from Table 17 for N_X in Equation 1 above to calculate the Uncorrected 90% CL upper limit branching ratios. I also used the systematic error corrected value of N_X, using Equation 3 above, to calculate the Corrected 90% CL upper limit branching ratios. The final results for both the uncorrected and corrected branching ratios, along with the 2000 PDG values, are given in Table 18. (Also see Figure 16).

Table 18: 90% CL Upper Limit Branching Ratios

Mode	Uncorrected BR	Corrected BR	BR (2000 PDG)
$D^0 \to \pi^+\pi^-\mu^+\mu^-$	2.95×10^{-5}	2.99×10^{-5}	
$D^0 \to \pi^+\pi^-e^+e^-$	3.56×10^{-4}	3.73×10^{-4}	
$D^0 \to \pi^+\pi^-\mu^\pm e^\mp$	1.44×10^{-5}	1.45×10^{-5}	
$D^0 \to K^-\pi^+\mu^+\mu^-$	1.63×10^{-4}	1.68×10^{-4}	
$D^0 \to K^-\pi^+e^+e^-$	2.70×10^{-4}	2.88×10^{-4}	
$D^0 \to K^-\pi^+\mu^\pm e^\mp$	2.31×10^{-4}	2.38×10^{-4}	
$D^0 \to K^+K^-\mu^+\mu^-$	3.26×10^{-5}	3.32×10^{-5}	
$D^0 \to K^+K^-e^+e^-$	2.98×10^{-4}	3.15×10^{-4}	
$D^0 \to K^+K^-\mu^\pm e^\mp$	1.67×10^{-4}	1.75×10^{-4}	
$D^0 \to \rho^0\mu^+\mu^-$	2.18×10^{-5}	2.20×10^{-5}	2.3×10^{-4}
$D^0 \to \rho^0e^+e^-$	1.21×10^{-4}	1.24×10^{-4}	1.0×10^{-4}
$D^0 \to \rho^0\mu^\pm e^\mp$	6.45×10^{-5}	6.56×10^{-5}	4.9×10^{-5}
$D^0 \to \overline{K}^{*0}\mu^+\mu^-$	2.54×10^{-5}	2.75×10^{-5}	11.8×10^{-4}
$D^0 \to \overline{K}^{*0}e^+e^-$	4.84×10^{-5}	5.29×10^{-5}	1.4×10^{-4}
$D^0 \to \overline{K}^{*0}\mu^\pm e^\mp$	8.31×10^{-5}	9.43×10^{-5}	1.0×10^{-4}
$D^0 \to \phi\mu^+\mu^-$	2.74×10^{-5}	3.04×10^{-5}	4.1×10^{-4}
$D^0 \to \phi e^+e^-$	5.07×10^{-5}	5.75×10^{-5}	5.2×10^{-5}
$D^0 \to \phi\mu^\pm e^\mp$	4.01×10^{-5}	4.53×10^{-5}	3.4×10^{-5}
$D^0 \to \pi^-\pi^-\mu^+\mu^+$	2.85×10^{-5}	2.88×10^{-5}	
$D^0 \to \pi^-\pi^-e^+e^+$	1.10×10^{-4}	1.12×10^{-4}	
$D^0 \to \pi^-\pi^-\mu^+e^+$	7.76×10^{-5}	7.86×10^{-5}	
$D^0 \to K^-\pi^-\mu^+\mu^+$	3.80×10^{-4}	3.90×10^{-4}	
$D^0 \to K^-\pi^-e^+e^+$	1.99×10^{-4}	2.06×10^{-4}	
$D^0 \to K^-\pi^-\mu^+e^+$	2.14×10^{-4}	2.18×10^{-4}	
$D^0 \to K^-K^-\mu^+\mu^+$	9.08×10^{-5}	9.40×10^{-5}	
$D^0 \to K^-K^-e^+e^+$	1.45×10^{-4}	1.52×10^{-4}	
$D^0 \to K^-K^-\mu^+e^+$	5.49×10^{-5}	5.68×10^{-5}	

1 J. Rasmunssen and A. Schwartz, *A Search for Rare and Forbidden* D^0, D^+, *and* D_s *Decays in FNAL E791*, (Offline_doc_234) September 10, 1997;
D. Sanders, *Search for Rare and Forbidden Dilepton Decays of* D^+, D_s^+ *and* D^0, (Offline_doc_393) May 19, 1999·

2 E. M. Aitala, *et al*., *Search for the Flavor-Changing Neutral-Current Decays* $D^+ \to \pi^+ \mu^+ \mu^-$ *and* $D^+ \to \pi^+ e^+ e^-$, Phys. Rev. Lett. **76**, 364 (1996).

3 E. M. Aitala, *et al*., *Search for Rare and Forbidden Dilepton Decays of the* D^+, D_s^+, *and* D^0 *Charmed Mesons*, Phys. Lett. **B462**, 401 (1999).

4 C. Zhang, *Muon ID Study using* $D^+ \to \overline{K}^{*0} \mu^+ \nu$ *mode*, (Offline_doc_219) November 2, 1995

5 L. Cremaldi, *Čerenkov ID Midplane Study*, (Offline_doc_317) August 1996.

6 N. Witchey, N. W. Reay, and A. Nguyen, *Muon Wall Efficiencies*, (Offline_doc_113) November 4, 1994.

7 G. J. Feldman and R. D. Cousins, *A Unified Approach to the Classical Statistical Analysis of Small Signals*, Phys. Rev. **D57**, 3873-3889 (1998).

8 R. D. Cousins and V. L. Highland, *Incorporating systematic uncertainties into an upper limit*, Nucl. Inst. Meth. **A320**, 331-335 (1992).

9 R. Sidwell, N. Stanton and N. Witchey, *Concise Technical Memo to Supplement FCNC PRL Draft#8*, (Offline_doc_417) April 5, 1995.

10 P. Gagnon, P. Burchat and P. Kasper, *Electron Identification in the E791 Offline Reconstruction Code*, (Offline_doc_88) April 1993.

Figures

Flavor-Changing Neutral-Current Modes

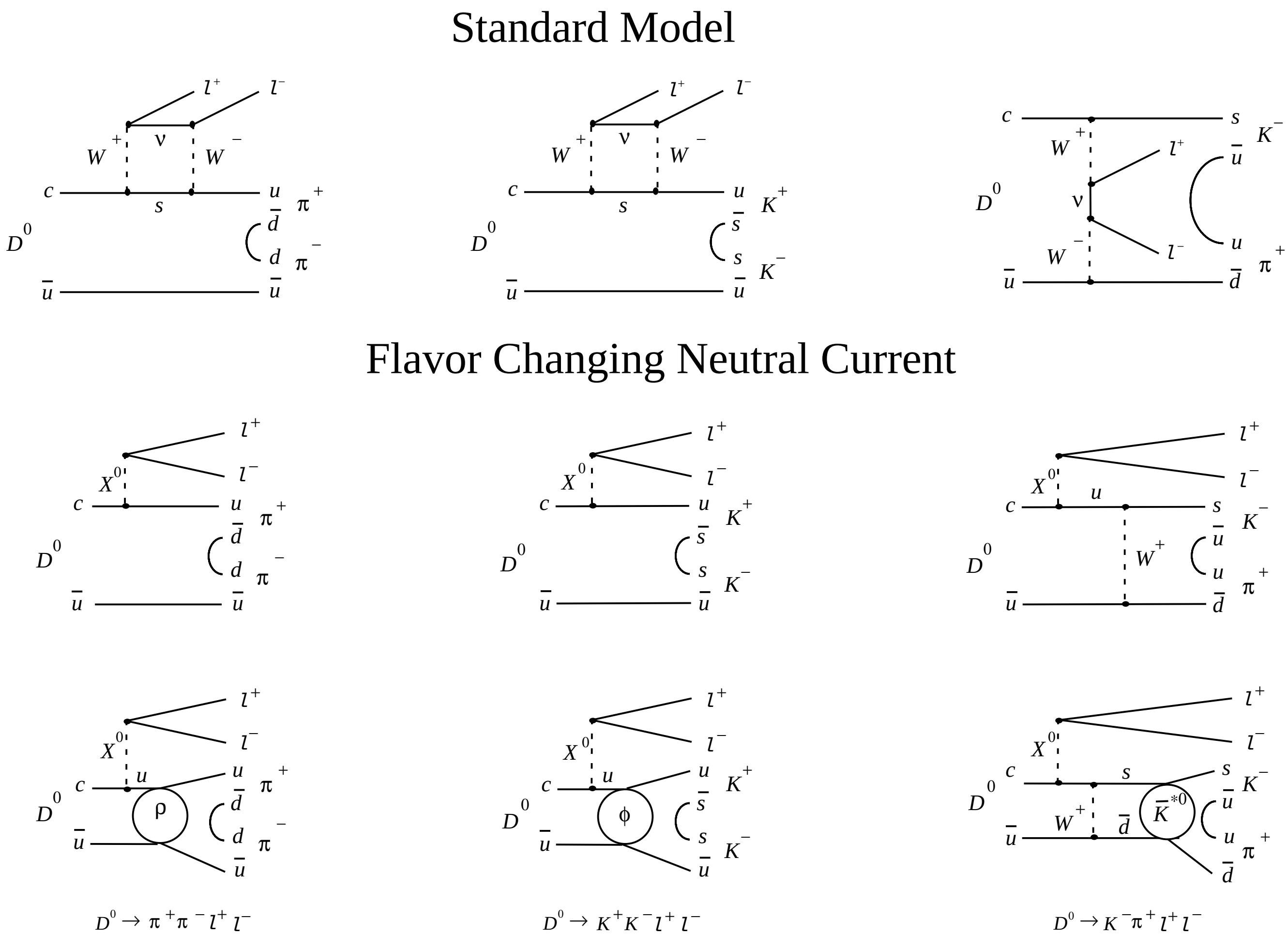

Figure 1:
Feynman Diagrams for FCNC decays.

Lepton Flavor Violating Modes

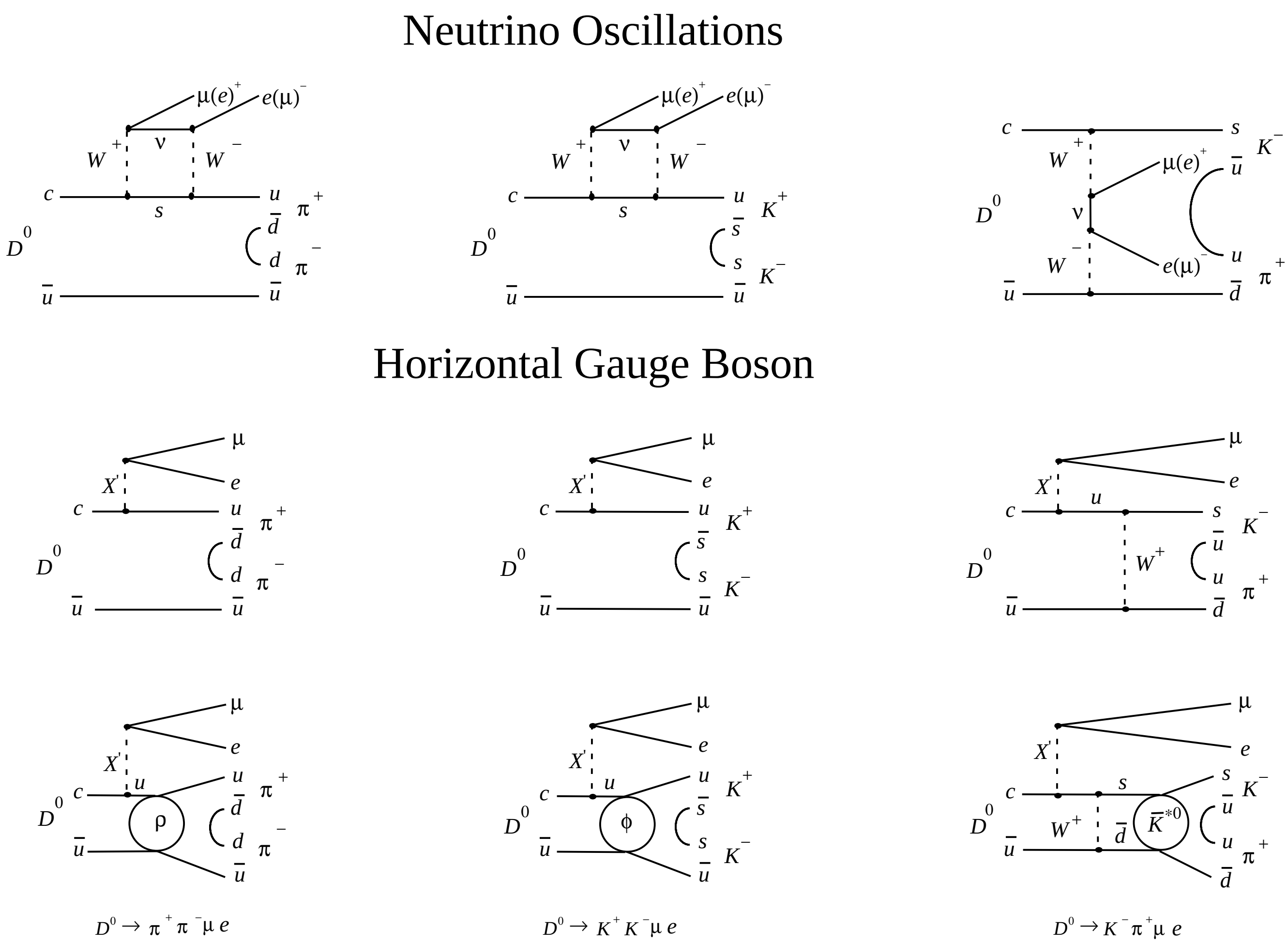

Figure 2:
Feynman Diagrams for LFV decays.

Lepton Number Violating Modes

Lepto-quark

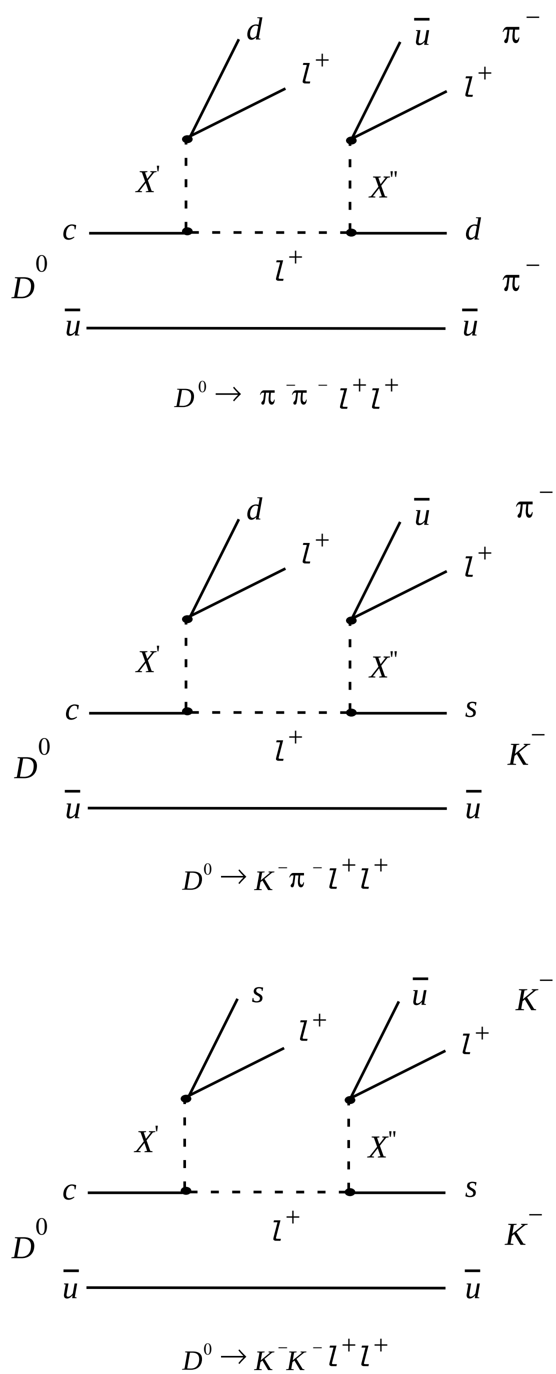

Figure 3:
Feynman Diagrams for LNV decays.

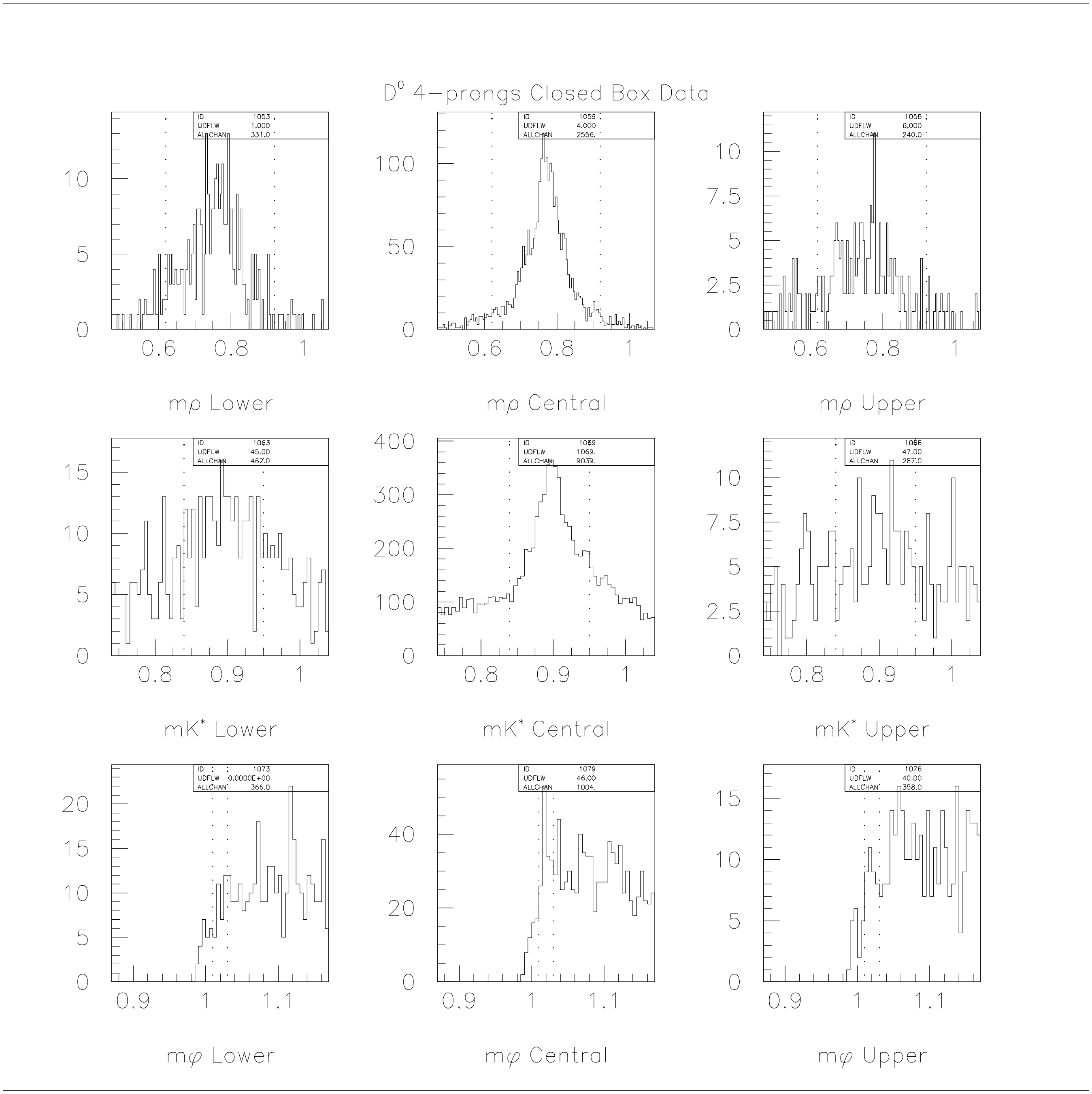

Figure 4:
Resonant masses for the normalization modes $D^0 \to \rho\pi^+\pi^-$ (top row), $D^0 \to \overline{K}^{*0}\pi^+\pi^-$ (middle row), and $D^0 \to \phi\pi^-\pi^+$ (bottom row). The dotted lines are the *rmass* cuts.
Bin width = 5 MeV/c^2.

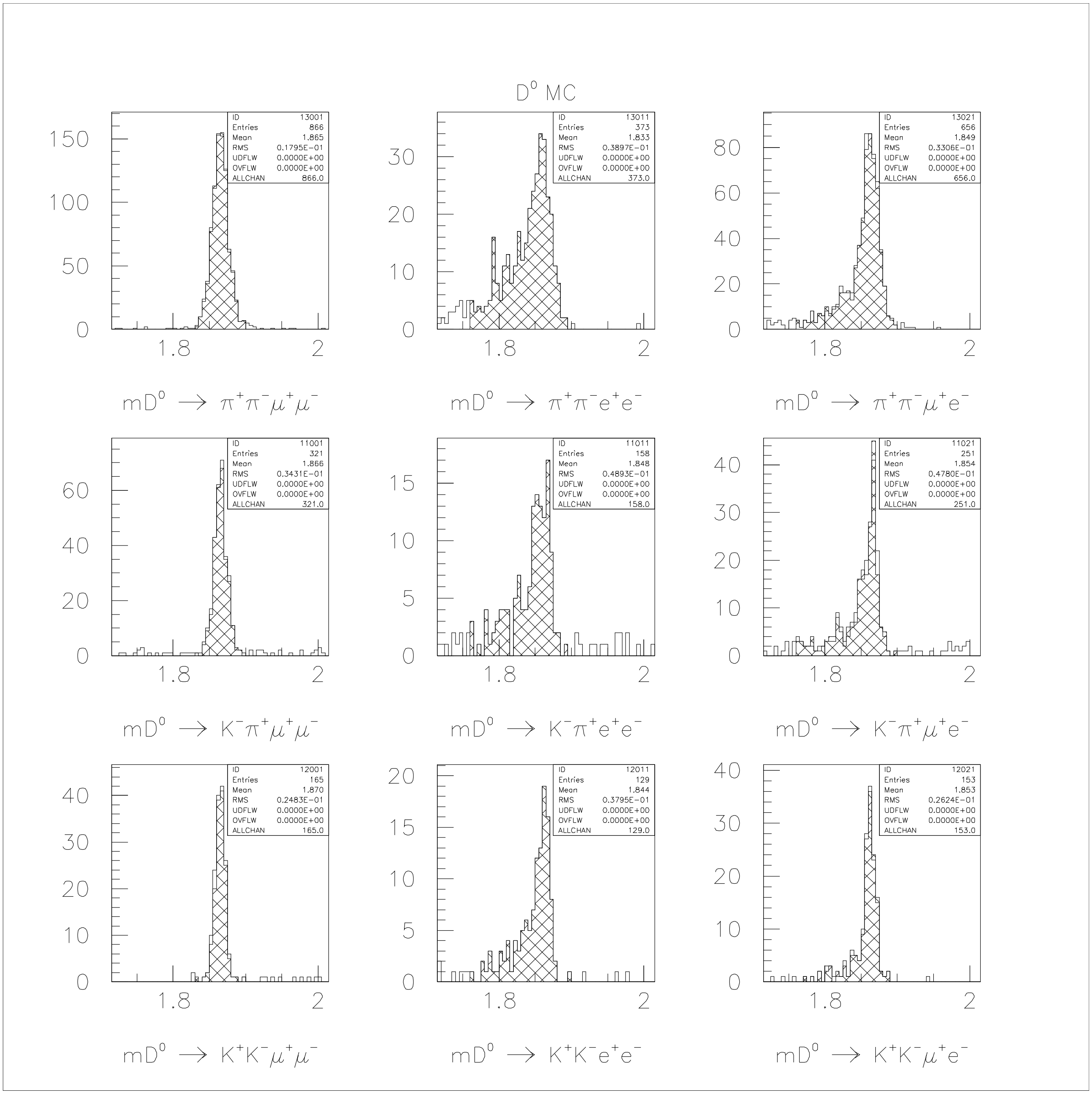

Figure 5:
Monte Carlo non-resonant dilepton decay modes. The crosshatched area is in the “box”.
Bin width = 5 MeV/c^2.

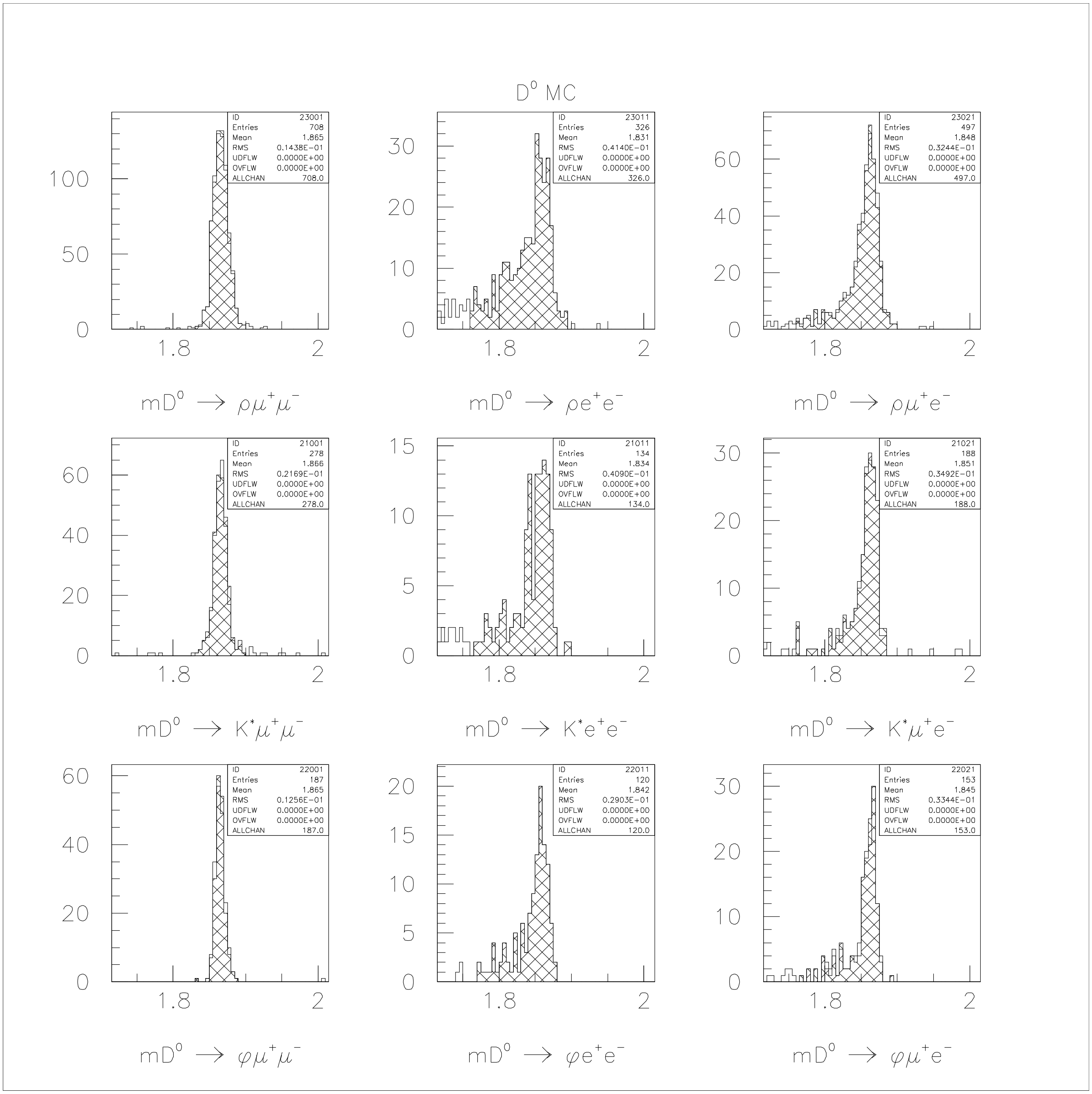

Figure 6:
Monte Carlo resonant dilepton decay modes. The crosshatched area is in the “box”.
Bin width = 5 MeV/c^2.

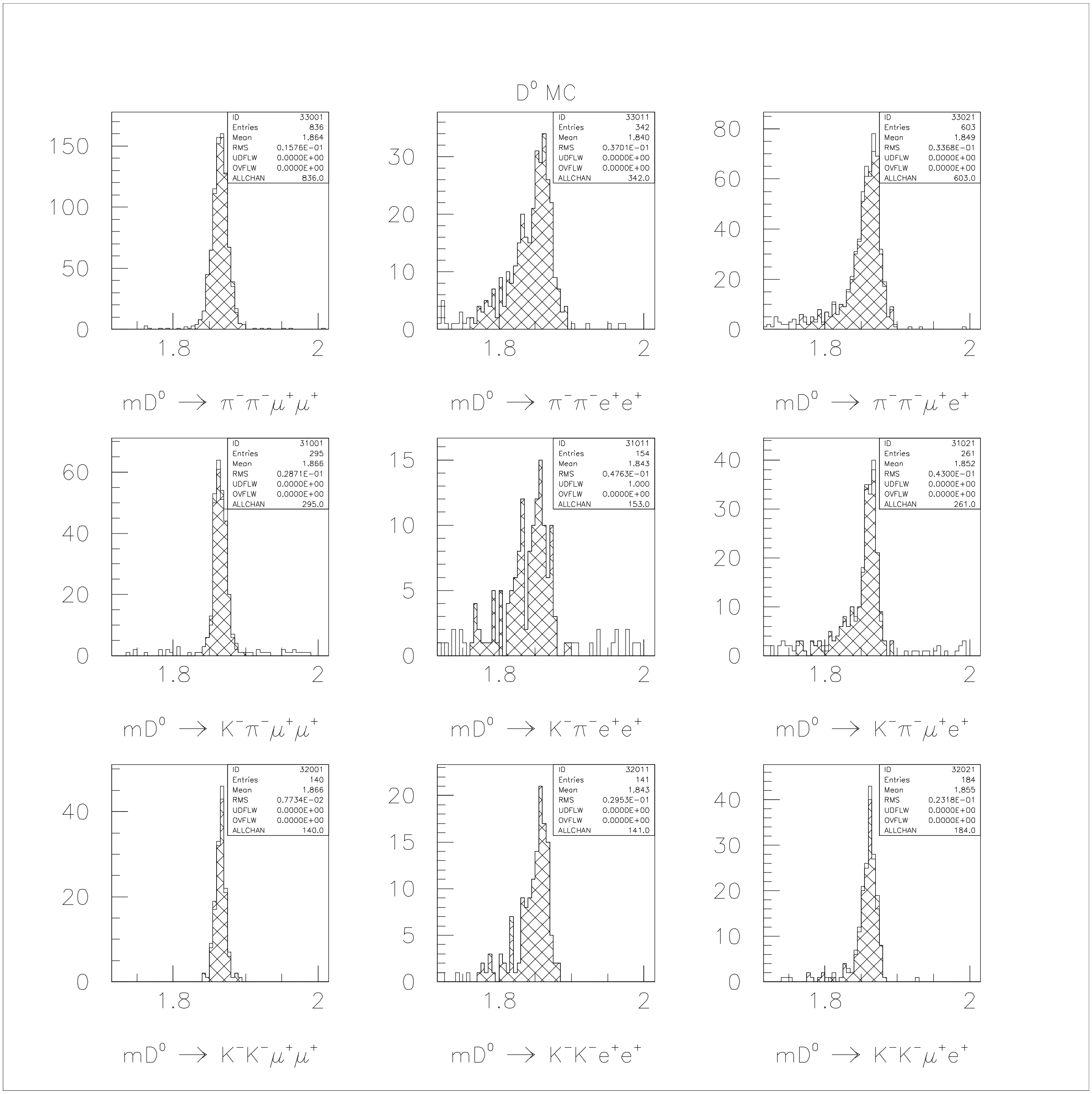

Figure 7:
Monte Carlo same-sign dilepton decay modes. The crosshatched area is in the “box”.
Bin width = 5 MeV/c^2.

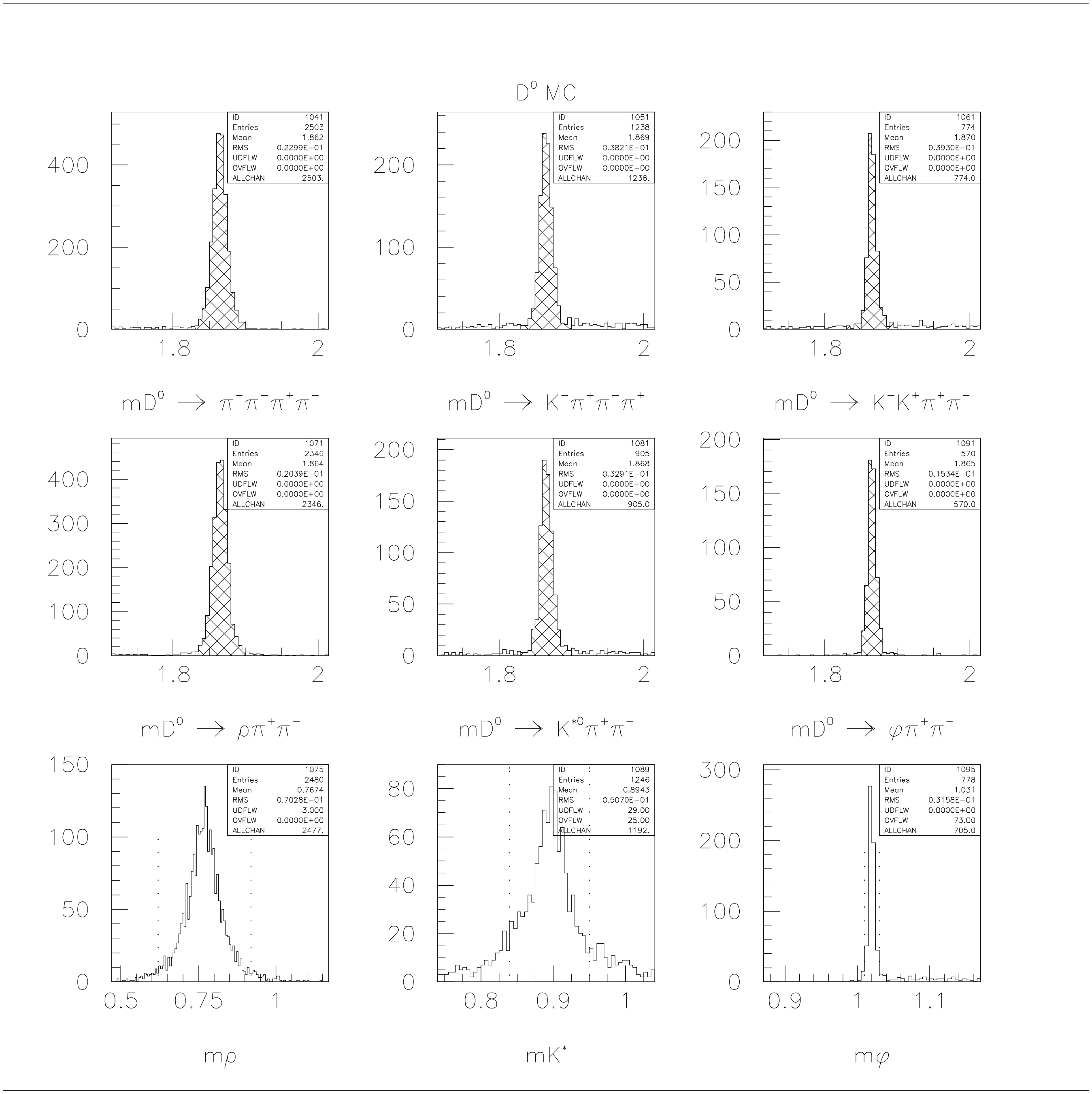

Figure 8:
Monte Carlo normalization modes. Non-resonant modes (upper row), resonant modes (middle row), and the resonant masses used in the middle row (bottom row). The crosshatched area is in the “box”. Bin width = 5 MeV/c^2.

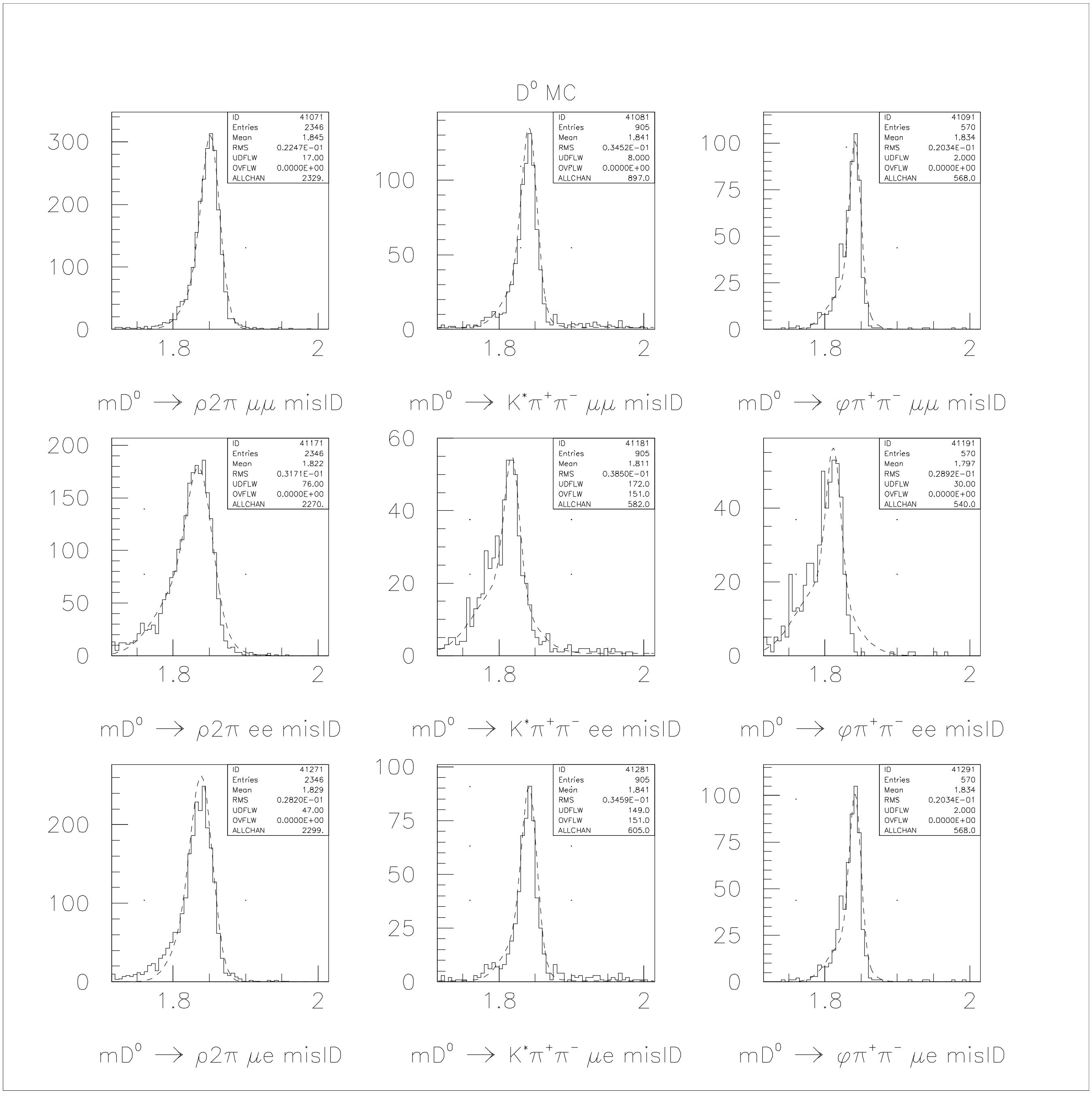

Figure 9:
Monte Carlo normalization modes with 2 pions misidentified as muons or as electrons.
The $\mu\mu$ (top row), *ee* (second row), and μe (third row) misidentified resonant modes are shown, along with the functional fits that were used. Bin width = 5 MeV/c^2.

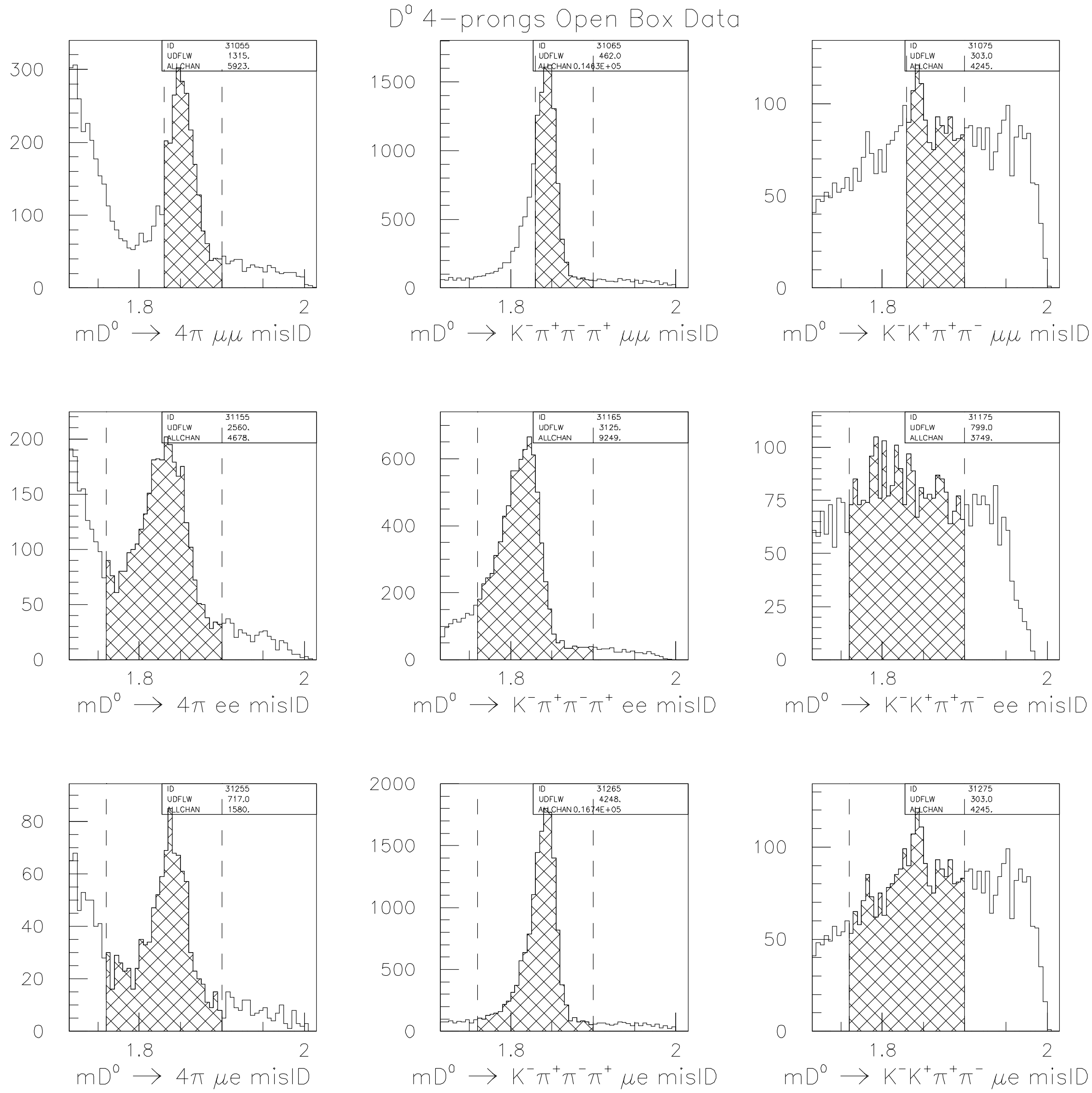

Figure 10:
Data normalization non-resonant modes with 2 pions misidentified as muons or as electrons. The $\mu\mu$ (top row), *ee* (second row), and μe (third row) misidentified modes are shown The crosshatched area is in the “box”. Bin width = 5 MeV/c^2.

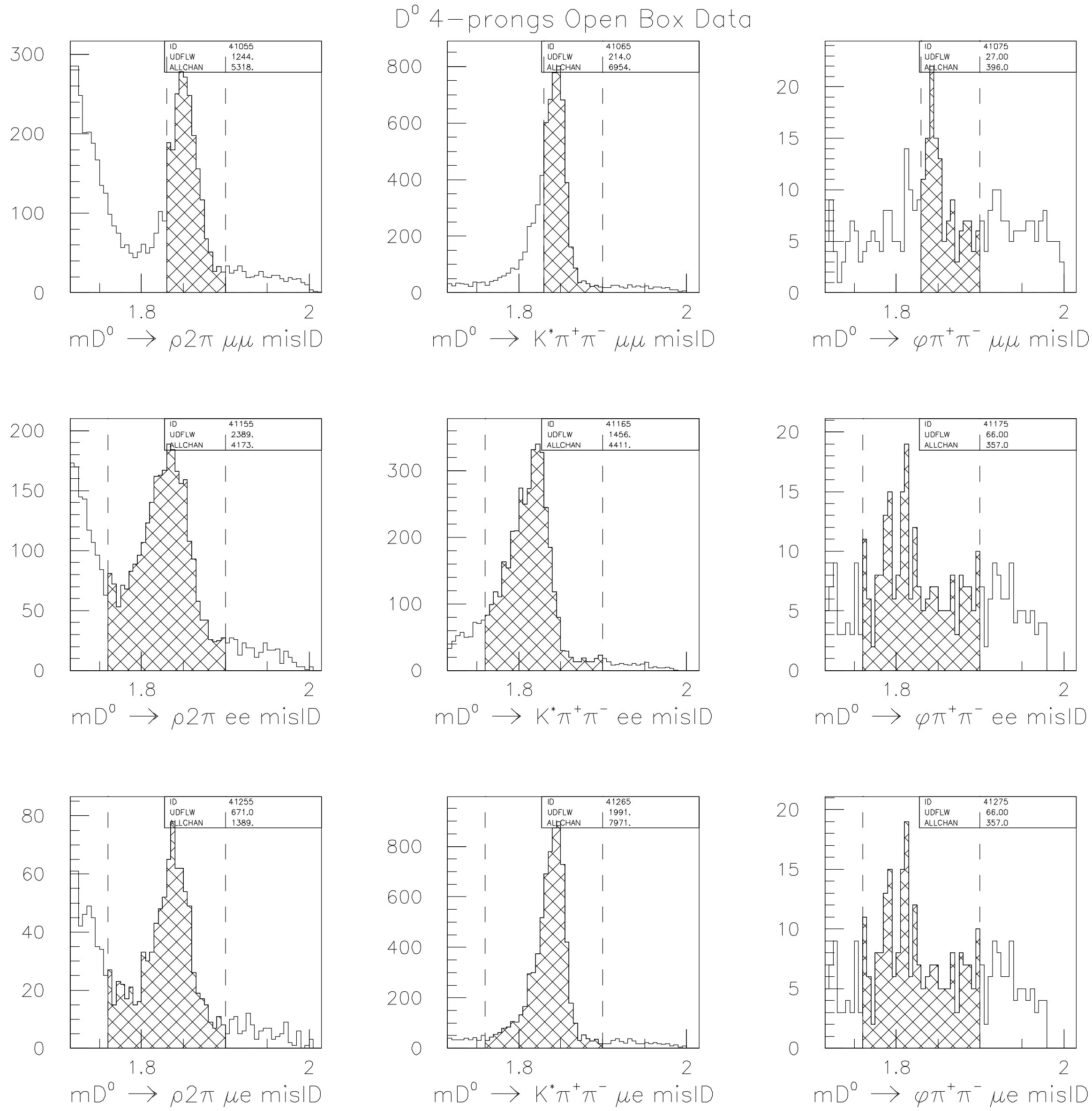

Figure 11:
Data normalization resonant modes with 2 pions misidentified as muons or as electrons. The $\mu\mu$ (top row), *ee* (second row), and μe (third row) misidentified modes are shown The crosshatched area is in the "box". Bin width = 5 MeV/c^2.

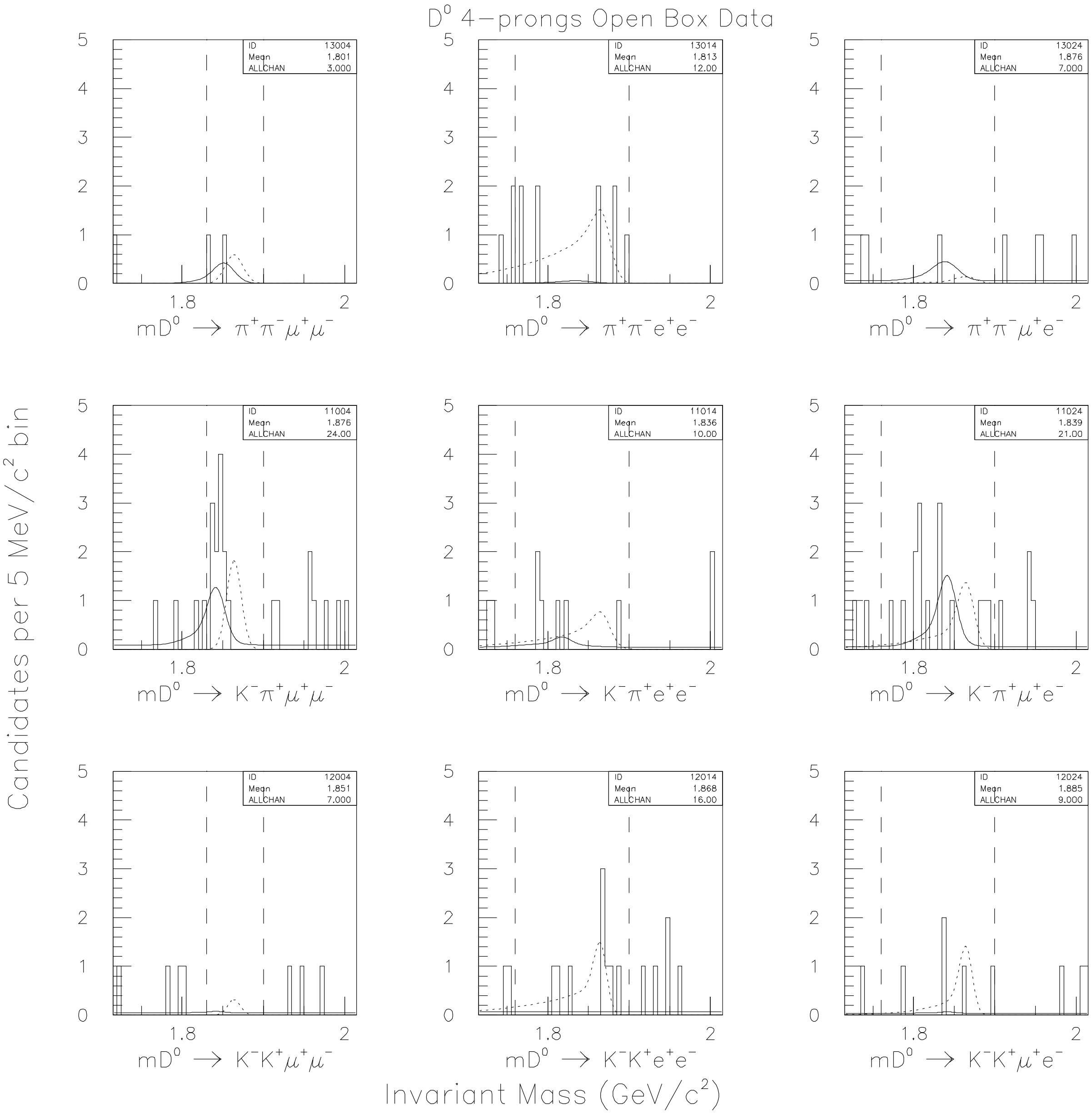

Figure 12:
Dilepton decay modes with no cut on the resonant mass. The solid line is the background shape.
The dotted line is the shape of the 90% CL upper limit number of events.
The dashed lines are the “box” boundaries.

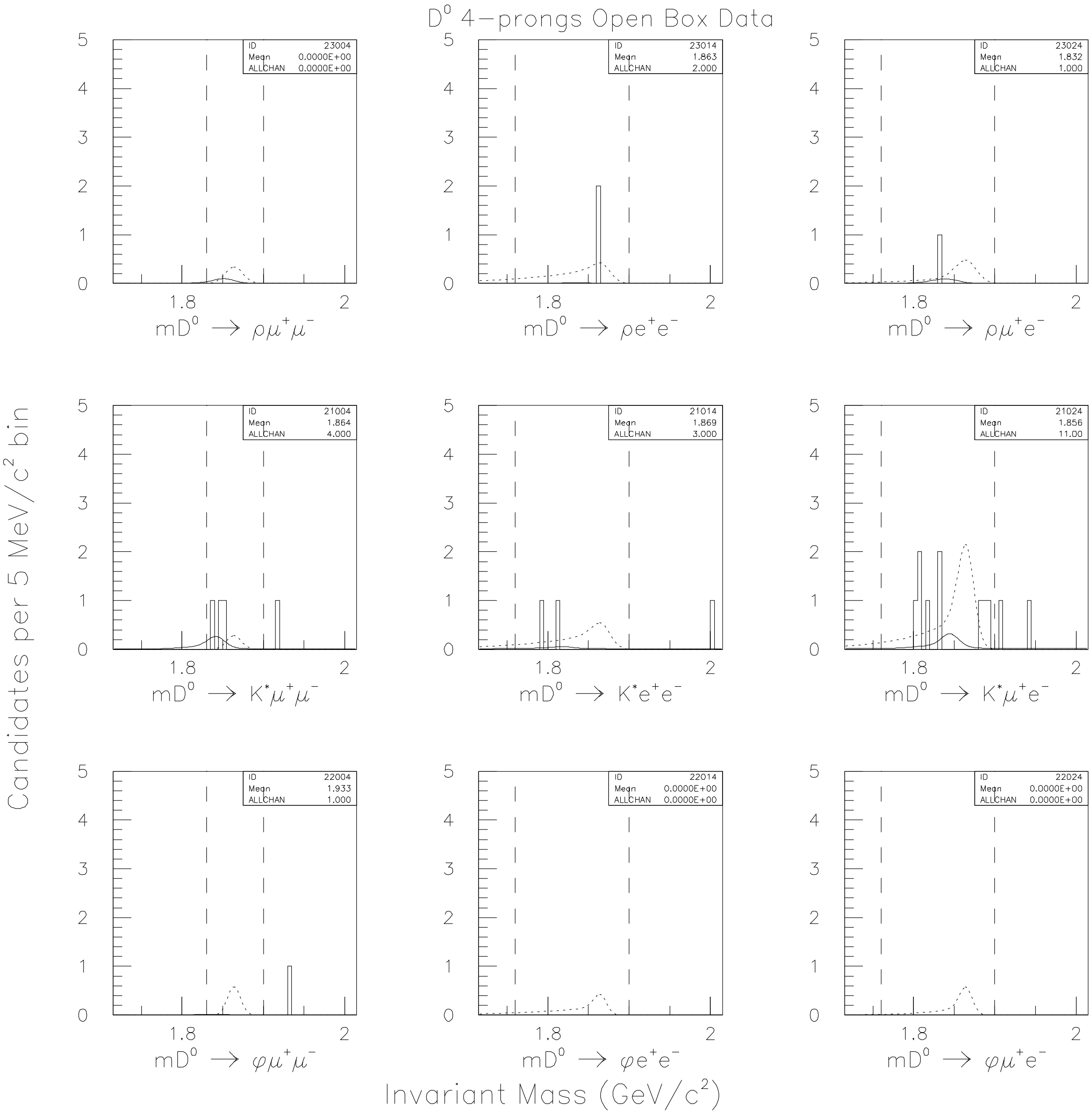

Figure 13:
Dilepton decay modes with the resonant mass cut. The solid line is the background shape.
The dotted line is the shape of the 90% CL upper limit number of events.
The dashed lines are the “box” boundaries.

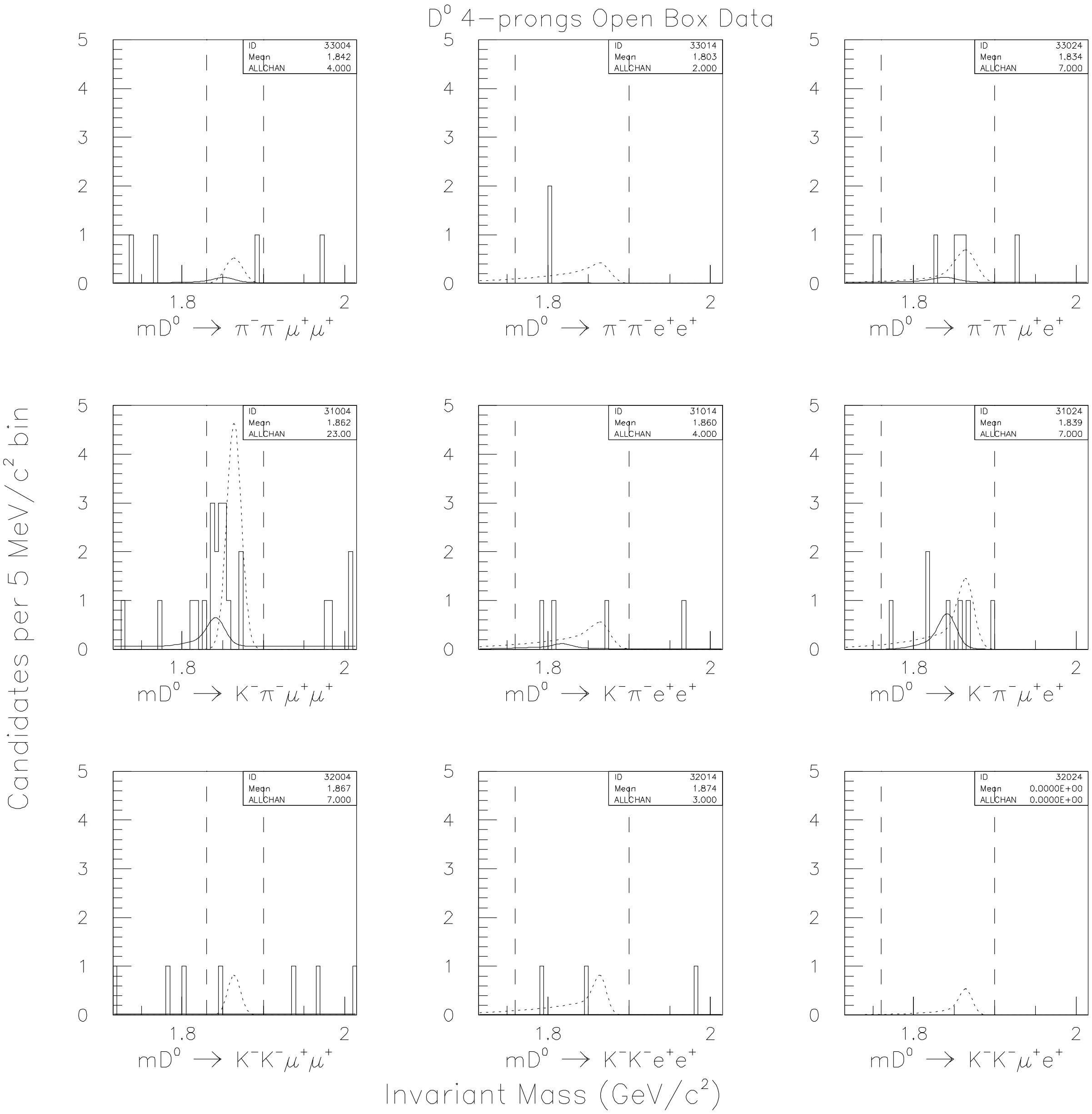

Figure 14:
Same-sign dilepton decay modes. The solid line is the background shape. The dotted line is the shape of the 90% CL upper limit number of events. The dashed lines are the “box” boundaries.

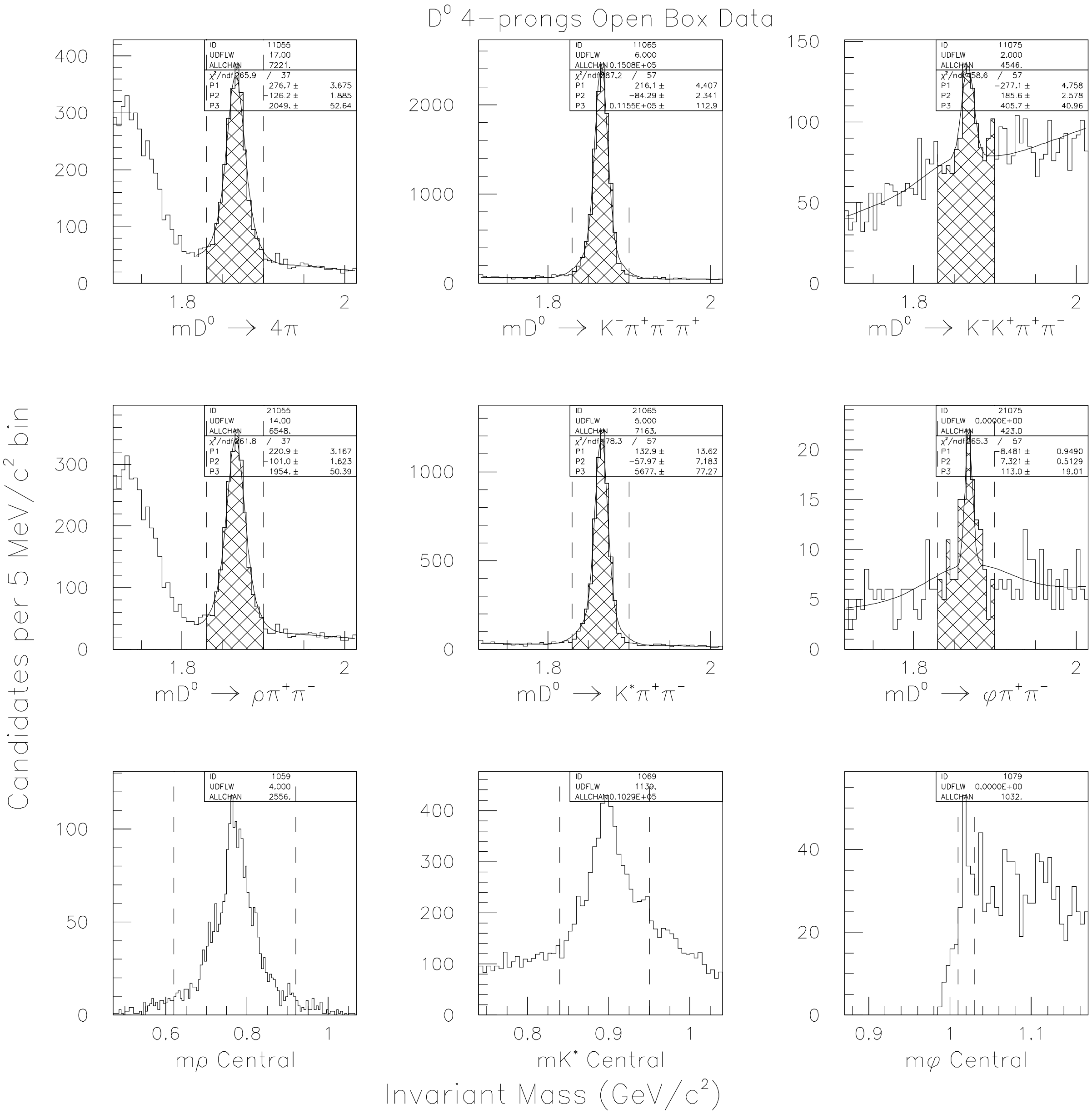

Figure 15:
Fitted data normalization modes. Non-resonant modes (upper row), resonant modes (middle row), and the resonant masses used in the middle row (bottom row).

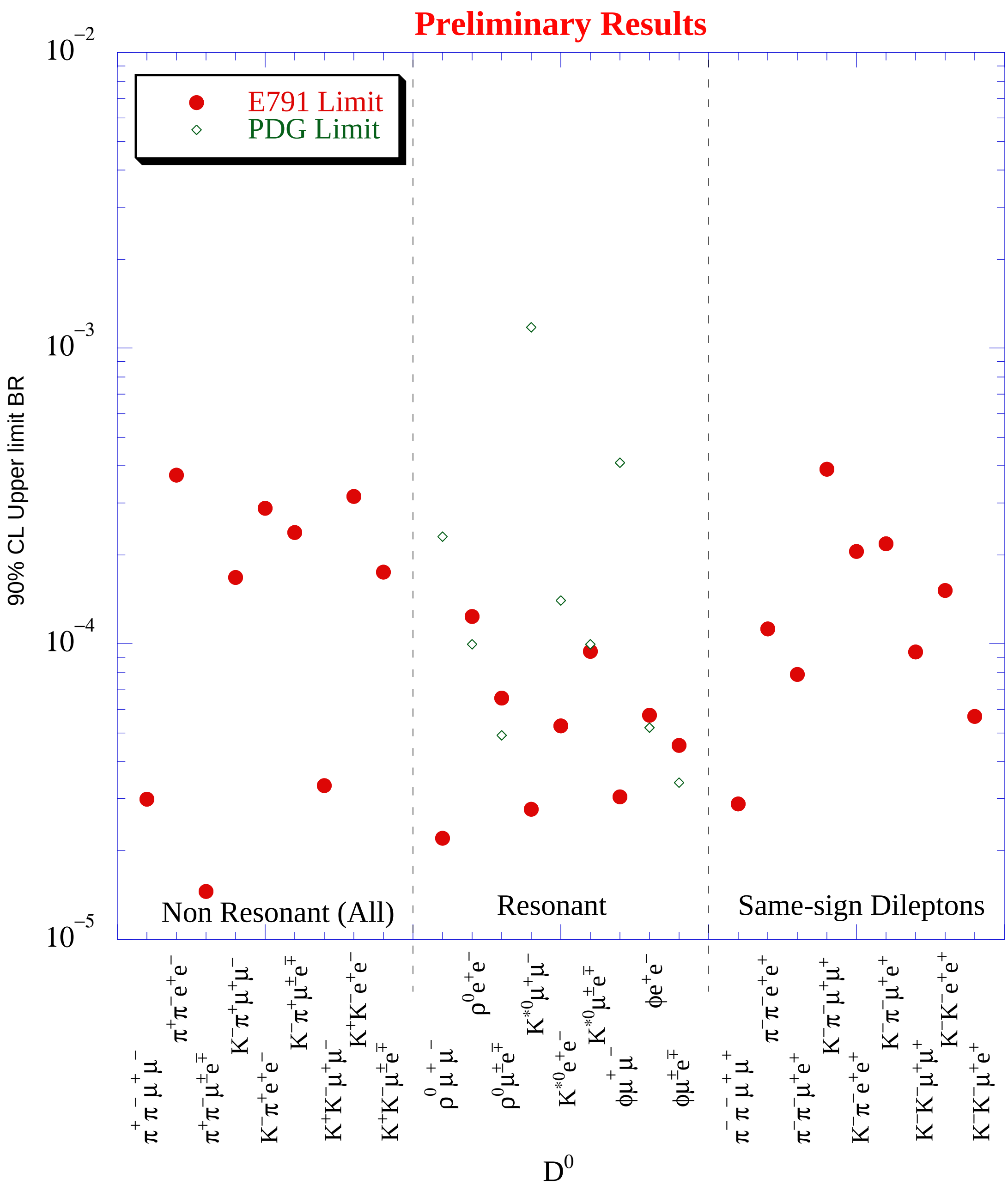

Figure 16: Preliminary results.